

¹ Crustal earthquakes in the Cook Inlet and Susitna region of southern Alaska

² Vipul Silwal^a, Carl Tape^a, Anthony Lomax^b

³ ^a*Geophysical Institute, University of Alaska, Fairbanks, USA*

⁴ ^b*ALomax scientific, Mouans-Sartoux*

⁵ **Abstract**

Several large ($M \geq 6$) earthquakes have occurred in the vicinity of Anchorage, Alaska, within the past century. The presence of the underlying subducting Pacific plate makes it difficult to determine the origin of these older earthquakes as either crustal, slab, or the subduction plate interface. We perform a seismological study of historical and modern earthquakes within the Cook Inlet and Susitna region, west of Anchorage. We first estimate hypocenters for historical large earthquakes in order to assess the likelihood as crustal, slab, or plate interface. We then examine modern crustal seismicity to better understand the style of faulting and the location of active structures, including within (and beneath) Cook Inlet and Susitna basins. We perform double-couple moment tensor inversions using high frequency body waves (1–10 Hz) for small to moderate ($M \geq 2.5$) crustal earthquakes (depth ≤ 30 km) occurring from 2007 to 2017. Our misfit function combines both waveforms differences as well as first-motion polarities in order to obtain reliable moment tensor solutions. Three focus regions—Beluga, upper Cook Inlet, and Susitna—exhibit predominantly thrust mechanisms for crustal earthquakes, indicating an overall compressive regime within the crust that is approximately consistent with the direction of plate convergence. Mechanisms within upper Cook Inlet have strike directions aligned with active anticlines previously identified in Cook Inlet from active-source seismic data. Our catalog of moment tensors is helpful for identifying and characterizing subsurface faults from seismic lineaments and from faults inferred from subsurface images from active-source seismic data.

⁶ **1. Introduction**

⁷ The active tectonics of south-central Alaska is governed primarily by the northwestern subduction of the
⁸ Pacific plate beneath the North America plate (Figure 1). The setting is one of the most seismically active
⁹ regions in the world, having produced the M_w 9.2 1964 earthquake. It includes pervasive earthquakes in the
¹⁰ slab, down to depths of 200 km, as well as crustal seismicity spanning a broad zone of intraplate deformation
¹¹ (Figure 2) [1, 2]. Many of the earthquakes—both large and small—are not clearly associated with any
¹² geologically mapped active faults. With improved locations of earthquakes and improved characterization

Email addresses: vsilwal@alaska.edu (Vipul Silwal), ctape@alaska.edu (Carl Tape), anthony@alomax.net (Anthony Lomax)

13 of the style of faulting from these earthquakes, we can better assess the active faults in the region. Here
14 we perform a seismological study of a tectonically complex region of south-central Alaska to improve our
15 understanding of active tectonics and seismic hazards in the region.

16 The Pacific plate subducts to the northwest under south-central Alaska (Figure 1a). Attached to the
17 Pacific plate to the east is the Yakutat microplate, identified as an oceanic plateau that is colliding and
18 subducting beneath Alaska [3, 4, 5]. The subducting Pacific/Yakutat plate is interpreted to be responsible
19 for the extremely shallow angle of subduction ($< 5^\circ$), far inland, as well as for the lack of volcanism [4, 6].

20 We focus on the Cook Inlet and Susitna region, which spans the western margin of the Pacific/Yakutat
21 plate (Figure 1a). The region, outlined in Figure 1, contains several notable tectonic elements. The sub-
22 duction interface [7] exhibits a clear kink from a westward-dipping slab to a northwestern-dipping slab [8]
23 (Figure 1a). The interface ranges from a depth of 40 km in the southeast, beneath the Kenai peninsula,
24 to a depth of 100 km in the northwest, beneath the Alaska Range. The southeast corner also marks the
25 approximate downdip extent of the 1964 M_w 9.2 earthquake [9, 10]. Slow slip and tectonic tremor have been
26 identified on the deeper sections of the interface, from about 40 km to 80 km [11, 12, 13, 14]. The crustal
27 thickness inferred from receiver functions is \sim 30 km in the northern region [15], implying that these deeper
28 slow slip events would arise from contact with subcrustal mantle.

29 The dynamics of underlying subduction provide context for characterizing crustal structures and crustal
30 earthquakes, which are the target of this study. Within the Cook Inlet and Susitna region are two mapped
31 active faults: the Pass Creek fault and the Castle Mountain fault. The earliest reference of the Pass Creek
32 fault (PCF) appears in [16], who reported “some thousands of feet” (p. 36) of displacement across the fault.
33 [17] interpreted PCF as a thrust fault but marked it as poorly constrained. Using interferometric synthetic
34 aperture radar (InSAR) elevation data, [18] inferred PCF to be a northwest dipping thrust fault and that it
35 “appears likely that the scarp is a result of at least several surface-rupturing earthquake” (p. 1471). They
36 estimated the fault has a slip-rate of \sim 0.5mm/yr and has the potential of producing a $M_{6.9} \pm 0.3$ earthquake
37 if the complete 37 km of the fault plane ruptured.

38 The Castle Mountain and Lake Clark fault system extends 500 km, from Lake Clark in the southwest and
39 into the Talkeetna mountains to the northeast [19]. The fault was interpreted as a right-lateral strike-slip
40 fault [19, 20], but recent analyses have identified compressional structures across the fault, as well as a lack
41 of definitive lateral offset indicators [21]. The Susitna section of the fault is the only section classified as
42 active, based on geomorphic evidence [22]. A paleoseismic study by [23] used data from nine trenches along
43 the fault near Houston, Alaska. They identified four major earthquakes in the past 2800 years, indicating a
44 recurrence interval of \sim 700 years. The two largest historical earthquakes in the region, in 1933 and 1943,
45 appear to have occurred near, but not on, the fault [24]. Based on the Global Centroid Moment Tensor
46 catalog, which started in 1976 [25, 26], the largest earthquake on the fault in the past 40 years occurred in
47 the northeastern most section as a M_w 5.8 right-lateral earthquake in 1984.

48 Physiographically the Cook Inlet and Susitna region is marked by the presence of two major sedimentary
49 basins (Figure 3): the Cook Inlet basin south of the Castle Mountain fault, and the Susitna basin north of
50 the fault (Figure 1b)). These basins are surrounded by mountains: Talkeetna mountains to the east, Alaska
51 Range to the northwest, Tordrillo mountains to the west, and Kenai mountains to the south. Additional
52 faults and folds have been identified within 3D active-source seismic data in Cook Inlet and Susitna basins
53 [27, 28, 18].

54 We conduct a seismological study that spans three different methods and three sets of earthquakes in the
55 Cook Inlet and Susitna region. First, in Section 2 we estimate the hypocenters of the largest earthquakes
56 ($M_w \geq 5.8$) that have occurred since the start of the instrumental era in 1904 [29]. We use globally recorded
57 arrival times of P and S waves, in addition to traveltimes predictions in a spherically symmetric Earth model,
58 within a probabilistic inversion for hypocenter and origin time. Second, in Section 3 we use P waveforms
59 and first-motion polarities to estimate focal mechanisms for crustal earthquakes $M_w \geq 2.5$. This procedure
60 is challenging on account of the lack of large earthquakes that are available. Third, in Section 4 we relocate
61 seismicity ($M \geq 1.5$, 1990–2017) using arrival time data and a double-difference relocation algorithm [30].
62 The results from these three analyses reveal a predominance of thrust faulting in the crust, consistent
63 with structural inferences from subsurface images, but differing from the strike-slip mechanisms previously
64 estimated from large historical earthquakes. Widespread seismicity and different styles of faulting provide
65 challenges for characterizing different scenarios for future large earthquakes in this region.

66 2. Hypocenter estimation of historical earthquakes

67 At least 12 major events ($M_w \geq 5.8$) have occurred in the Cook Inlet and Susitna region since the
68 start of instrumental era in 1904. Table 2 summarizes previous publications of the magnitudes for these
69 earthquakes. For larger earthquakes we use the Global Centroid Moment Tensor (GCMT) catalog [25, 26]
70 for events since 1976 and the ISC-GEM catalog [31, 32] for events before 1976. The ISC-GEM catalog
71 provides relocated hypocenters [33, 34] and magnitude estimates [35]. In recent years, it has expanded its
72 coverage of historical earthquakes to lower magnitudes. Doser and colleagues have estimated hypocenters,
73 magnitudes, and mechanisms for many historical earthquakes in south-central Alaska [36, 37, 24, 38].

74 Depth estimates of the hypocenters and of the subduction interface provide a starting point for interpreting
75 the earthquakes as either crustal, interface, or intraslab. Table 3 reveals a mix of crustal and intraslab (or
76 interface) earthquakes. Interestingly, the occurrence of earthquakes in the crust versus slab appears to have
77 changed with time, as shown in Figure 4. Prior to 1950 most earthquakes were crustal; after 1950 all four
78 earthquakes were in the slab. This pattern was previously noted [24] and is apparent within a larger region.
79 [24] speculated that 1964 $M_w 9.2$ earthquake was responsible in the shift from crustal to slab earthquakes.

80 We use a nonlinear probabilistic approach to estimate the hypocenters of the 11 pre-1976 earthquakes

⁸¹ $M_w \geq 5.8$ in the region (Table 2). The code, NonLinLoc, uses an efficient global sampling algorithm to
⁸² obtain an estimate of the probability density function (pdf) in 3D space for the hypocenter location [39].
⁸³ The pdf (and the likelihood) is computed using the misfit between the observed and theoretical arrival times
⁸⁴ for teleseismic stations. Theoretical travel times are computed for spherical earth with ak135 velocity model
⁸⁵ [40] using the TauP Toolkit [41]. Recorded arrival times are obtained from the International Seismological
⁸⁶ Centre [42].

⁸⁷ Our full results for all 11 historical earthquakes are presented in [43]; next we highlight three of the
⁸⁸ largest earthquakes.

⁸⁹ *2.1. The 1933, 1943, and 1954 earthquakes*

⁹⁰ We present results from three $M_w > 6$ earthquakes in the Cook Inlet and Susitna region: 1933-04-27
⁹¹ M_w 6.8, 1943-11-03 M_w 7.3, and 1954-10-03 M_w 6.4 (Table 2). These earthquakes were widely felt across
⁹² south-central Alaska, including Kodiak, to the southwest, and at least as far north as Fairbanks, which is
⁹³ about 400 km from the epicenters. Appendix A summarizes felt reports of these earthquakes. The 1933
⁹⁴ earthquake toppled telegraph lines around Anchorage, broke storefront windows in Anchorage, and shook
⁹⁵ houses off foundations in Old Tyonek. The 1954 earthquake produced minor landslides over the highway,
⁹⁶ damaged a section of railroad, and damaged structures in Anchorage and the western Kenai peninsula.
⁹⁷ Although having the largest magnitude of the three earthquakes, the 1943 earthquake did not lead to any
⁹⁸ reported damage in the region. By comparison, the maximum shaking intensities in Anchorage—which
⁹⁹ is approximately equidistant from the three earthquakes—were MMI 6 (1933), MMI 5 (1943), and MMI 8
¹⁰⁰ (1954) (Appendix A; [44]). These discrepancies could arise from influences of 3D structure on ground motion,
¹⁰¹ from source effects (radiation pattern or directivity), and from possible inconsistencies in the MMI values
¹⁰² (e.g., are the MMI values from the same place in Anchorage?).

¹⁰³ The seismicity cross sections in Figure 2b-c provide context for these three earthquakes. The plots show
¹⁰⁴ our maximum likelihood (MLL) hypocenters for the three earthquakes in the context of modern seismicity
¹⁰⁵ and estimated subsurface interfaces (subduction and Moho). From these results alone, it appears that the
¹⁰⁶ 1933 and 1943 earthquakes are crustal, while the 1954 earthquake was likely intraslab, though we cannot
¹⁰⁷ rule out the subduction interface as a possibility (Table 3). We discuss this further in Section 5.3.

¹⁰⁸ Station coverage and traveltimes residuals for our MLL hypocenters (and origin times) are shown in Fig-
¹⁰⁹ ure 5. Figure 6 shows our posterior epicenters for the three earthquakes. These ‘clouds’ are approximately
¹¹⁰ 30 km by 40 km and convey the uncertainty associated with the epicenter estimation. For each posterior
¹¹¹ hypocenter we calculate its vertical distance to the subduction interface, and these differences are then plot-
¹¹² ted as histograms in the bottom row of Figure 7. These distributions provide critical uncertainties for the
¹¹³ interpretation of the earthquakes as crustal, subduction interface, or intraslab. For example, Figure 7c (bot-
¹¹⁴ tom) makes the case for the 1954 earthquake as intraslab. (However, note that we do not have uncertainties

115 for the subduction geometry models, including the one we have chosen to use [7]).

116 3. Moment tensor inversions for modern crustal earthquakes

117 A double couple moment tensor is a 3×3 symmetric matrix whose eigenvalues are $(\lambda, 0, -\lambda)$. We are
118 concerned with estimating the magnitude and orientation (strike, dip, rake) of the moment tensor, which we
119 also refer to as the ‘source mechanism’. Alternative terms for double couple moment tensors are ‘fault-plane
120 solution or ‘focal mechanism.’ The strike, dip, and rake define the moment tensor orientation, as well as
121 one of the two possible fault planes.

122 Three catalogs of moment tensors are summarized in Figure 8: (a) [24]: large $M_w > 6$ historical (pre-
123 1964) earthquakes; (b) the GCMT catalog [25, 26]: post-1976 earthquakes, predominantly $M_w > 5.3$;
124 (c) crustal earthquakes from the Alaska Earthquake Center fault-plane catalog: predominantly $M_I > 3$. We
125 also considered the focal mechanism catalog of [7], which includes 117 earthquakes over a one-year period of
126 MOOS (2007–8). Almost all of these earthquakes are within the slab or to the southeast of our focus region.

127 Within the Cook Inlet and Susitna region, we see two historical crustal earthquakes (1933, 1943) and
128 zero crustal earthquakes since 1976 (GCMT: [25, 26]). There is one event in the GCMT catalog that is
129 ≤ 30 km depth, plotted as a red beachball near Anchorage in Figure 8b. The depth is listed as 15 km in the
130 GCMT catalog, but the Alaska Earthquake Center (AEC) earthquake catalog, using all available regional
131 data, lists 31 km for the depth, which would likely be an intraslab origin (not crustal) for the earthquake.
132 The GCMT magnitude of $M_w 5.3$ is near the completeness level for the catalog, which indicates that there
133 is limited global data for estimating the moment tensor. This might explain the large discrepancy between
134 the moment tensor from GCMT and the one from the Alaska Earthquake Center, as shown in Figure 6.

135 Focal mechanisms for crustal earthquakes since 1990 are available from Alaska Earthquake Center. The
136 mechanisms are estimated from first-motion polarities, and they vary widely across the region. Our primary
137 motivation was to use enhanced methods, including waveforms, and enhanced station coverage from the
138 past decade, to estimate moment tensors.

139 3.1. Event selection for moment tensor inversions

140 We consider earthquakes in the Cook Inlet and Susitna region shallower than 30 km and occurring
141 between 2007-08-15 and 2017-01-01. From the spatial distribution of crustal seismicity (Figure S10), we
142 identified three subregions to select events for moment tensor inversions: Beluga region, Upper Cook Inlet
143 region, and Susitna region (Table 1 and Figure S8). The time period of event selection, 2007–2017, spans
144 two seismic experiments in the region: MOOS (2007–2009) [7, 45] and SALMON (2015–2017) [46, 47] and
145 also includes new stations from the EarthScope Transportable Array (TA) in Alaska (2014–2019). Station
146 coverage is a primary factor on the reliability of our moment tensor solutions. Events in 2010, following the

147 end of MOOS, have poor station coverage. Events starting in 2015 have the best coverage due to SALMON
148 and TA networks.

149 We selected 53 events for moment tensor inversions: 9 from the Beluga region, 22 from the Upper Cook
150 Inlet region, and 22 from the Susitna region. Hypocenters and origin times were obtained from the AEC
151 catalog. These were fixed for the moment tensor inversions. Analyst-reviewed P arrival times and polarities
152 were used for stations in the permanent network (AK, AT, AV). For stations in temporary networks (MOOS,
153 SALMON, TA), we picked the P arrival times and assigned polarities.

154 *3.2. Moment tensor inversion method*

155 Estimating a moment tensor for an earthquake involves comparing observed waveforms with synthetic
156 waveforms calculated for an assumed moment tensor for an assumed model of Earth structure. We use the
157 same layered seismic velocity model used by the Alaska Earthquake Center for moment tensor inversions
158 and for locating earthquakes; see Table S1 of [48]. We use the ‘cut-and-paste’ approach to estimate moment
159 tensors for earthquakes [49, 50, 51]. In this approach, each three-component seismogram is cut into two body
160 wave windows and three surface wave windows. Different bandpass filters are applied to the body waves
161 and surface waves. The same procedures are applied to synthetic seismograms, which are then quantifiably
162 compared with the recorded seismograms, via a misfit function. As demonstrated in [48], the choices within
163 the misfit function can have a significant impact on the estimated best-fitting moment tensor. Our previous
164 studies [48, 52] employed a simplified treatment of first-motion polarities that is generalized here.

165 Within the grid-search moment tensor inversion, the synthetic seismograms are aligned with the observed
166 seismograms by applying time shifts to the synthetic waveforms that minimize the misfit between synthetic
167 and observed waveforms. In many cases, this minimization can result in time shifts that are unreasonable,
168 based on comparisons with a larger set of measurements. In these cases of cycle skipping, the synthetic
169 waveforms are aligned on the wrong portion of the observed waveforms. The challenges of cycle-skipping
170 and time shifts have been discussed previously [52, 53]. In our study we specify the observed P onset times,
171 which effectively eliminates the need for time shifts.

172 Figure 9 shows a moment tensor inversion result for one of 22 crustal earthquakes in the Susitna region.
173 Its relatively large magnitude (M_w 4.2) allows us to use surface waves, in addition to body waves. For
174 all the other events, only P waves (and P polarities) were used. The example shows the basic approach to
175 comparing recorded waveforms (black) with synthetic waveforms (red) generated using a layered Earth model
176 and a moment tensor source. Significant differences in shapes between data and synthetics are attributed
177 to complexities in 3D Earth structure that are unmodeled by the synthetics. For this event, the recorded
178 waveforms to the southwest exhibit are influenced by Cook Inlet basin, as well as by Susitna basin from
179 the source region. Some of these differences in structure between our assumed 1D model and real 3D Earth
180 structure are encapsulated by the time shift maps shown in Figure 9.

181 3.3. Misfit function

182 Small earthquakes ($M_w < 3.5$) do not produce large signals at low frequencies. Therefore we are forced
 183 to use higher frequency waveforms, which are sensitive to 3D structural heterogeneities. Most regional
 184 networks do not have enough stations to capture the detailed effects of 3D structure on the wavefield. As
 185 used in previous studies [54, 55, 56, 57], first-motion polarity measurements (i.e., up or down) can be used
 186 to stabilize the waveform misfit function. Below we define our misfit function that combines waveforms
 187 differences and polarity differences.

The L1-norm waveform misfit is given by

$$\Phi_w(M) = \sum_{j=1}^{N_s} \sum_{i=1}^5 \left[(\mathbf{u}_{ij} - \mathbf{s}_{ij}(M))^T \mathbf{W}_{ij} (\mathbf{u}_{ij} - \mathbf{s}_{ij}(M)) \right]^{1/2} \quad (1)$$

188 where N_s is the number of stations used, i is the window index for a seismogram, j is the station index for
 189 an event, \mathbf{u} is a discretized recorded seismogram, $\mathbf{s}(M)$ is a discretized synthetic seismogram for moment
 190 tensor M , \mathbf{W}_{ij} is a square weighting matrix with the same dimension as the number of time points. As
 191 discussed in Section S1, we choose \mathbf{W}_{ij} to be a constant-valued diagonal matrix with a weight factor that
 192 takes into account the duration of the time window, the width of the bandpass, and a user-specified weight.
 193 Recent approaches have considered non-diagonal weighting matrices based on estimated noise at each station
 194 [58, 59, 60].

The polarity misfit is given by

$$\Phi_p(M) = \frac{1}{2} \sum_{j=1}^{N_p} |p_j - t_j(M)| \quad (2)$$

195 where p is the observed polarity, t is the theoretical polarity for the moment tensor M , and N_p is the number
 196 of stations at which first-motion polarity is picked. p and t can either be +1 (up) or -1 (down), so that the
 197 polarity misfit for a station is either 0 or 1.

The total misfit is a weighted sum of the normalized waveform and polarity misfit

$$\Phi(M) = h(N_s) \left(m \frac{\Phi_p(M)}{N_p} + (1-m) \frac{\Phi_w(M)}{\|\mathbf{u}\|_{L1}} \right) \quad (3)$$

198 where the waveform misfit normalization $\|\mathbf{u}\|_{L1}$ is same as given in equation 7 of [48], m is the weight given
 199 to the polarity misfit, and $h(N_s)$ is the station reward factor (see Section S1). This misfit function was also
 200 used in [53, 61] for full moment tensor inversions.

201 The Supporting Information includes text and figures to illustrate the roles of different variables in the
 202 misfit function.

203 3.4. Results

204 Our moment tensor inversion results for 53 crustal earthquakes in three regions (Table 1) are presented in
 205 Tables S2–S4, in Figure 12, and in [62]. The regions exhibit predominantly thrust earthquake mechanisms

206 that are consistent with the plate convergence direction of 339° (N21W) [2]. Specifically, the T axis of
207 the mechanisms are near vertical, and the P axes of the mechanisms are near horizontal and point in the
208 northwest direction of plate convergence.

209 In Figure 11 we compare our moment tensor results, which use P waveforms and first-motion polarities,
210 with a catalog of mechanisms (AECfp) produced by the Alaska Earthquake Center that uses first-motion
211 polarities only (fpfit: [63]). For the time period 2007-08-15 to 2017-01-01 and depths ≤ 30 km, the AECfp
212 catalog contains 46 earthquakes, 26 of which were examined in our study. The additional earthquakes in
213 the AEC catalog were ones that were either not within our three regions or were excluded by us due to low
214 signal-to-noise levels for waveforms (Section 3.1). Therefore the comparison in Figure 11 is between a set
215 of 53 moment tensors derived from P waveforms and a set of 46 derived from P polarities. The result in
216 Figure 11a, which includes 27 that are not in (b), is a more coherent pattern of thrust faulting, whereas
217 Figure 11b is predominantly strike-slip faulting. This suggests that the inclusion of waveforms, as in our
218 study, may help discriminate among strike-slip and thrust mechanisms in cases where P polarities alone
219 cannot isolate the mechanism. Specifically, the moment tensor for a north-striking thrust fault dipping 45°
220 (west or east) can be rotated 90° about its P-axis; this will result in a strike-slip moment tensor that is
221 significantly overlapping with the original moment tensor (as quantified by $\omega = \angle(M_1, M_2) = 60^\circ$, which
222 is much less than the maximum of 180°). Although the mechanisms look different, they are not easily
223 constrained by seismic data, and a formal assessment of uncertainties could elucidate this point [48]. Of
224 course, better station coverage would also help discriminate between the strike-slip and thrust mechanisms.
225 By examining small, shallow earthquakes, we are unlikely to have the ray path coverage of the center of the
226 source mechanisms. Shallow events, the upward ray paths cover a small region of the surface, where
227 we are unlikely to have a station. For small events, the downward ray paths have too-small signal-to-noise
228 by the time they reach distant stations. Station coverage for the source mechanisms is best viewed in the
229 beachball plots in [62].

230 4. Hypocenter relocation of modern crustal seismicity

231 We apply the double-difference hypocenter relocation method of [30] to crustal seismicity in the Cook
232 Inlet and Susitna region. The double difference method relies on minimizing the difference between observed
233 and theoretical travel-times difference for pairs of earthquakes at each station. The method, especially when
234 used in conjunction with waveform cross correlations, has been effective in collapsing diffuse clouds of
235 seismicity onto strikingly sharp fault-like features; meanwhile other diffuse clouds remain diffuse [64, 65].
236 The changes in the locations are also used to reduce the systematic errors due to the model, which could be
237 used to improve the tomography models [66].

238 Our work expands on the results of [67], who relocated crustal earthquakes with $ml > 2.0$ and depths

≤ 50 km in southern Alaska occurring during 1988–1996 using the joint hypocenter determination (JHD) method [68]. They classified their results into five regions, one of which coincides with our target region: “Shallow North American intraplate earthquakes (0–25 km) located to the west of 149° W” (p. 96). Their results revealed diffuse seismicity within the crust.

We used a much larger data set, spanning from 1990-01-01 to 2017-01-01, and a more robust double-difference hypocenter relocation method [30]. We used crustal events (depth ≤ 30 km) with $M_I \geq 1.5$ occurring between 1990-01-01 and 2017-01-01 (Table 1). With these selection criteria, we started with 5726 events from the AEC catalog. The final relocated catalog, after removing 35 (depth > 40 km) events, contained 4748 earthquakes. The changes between the initial hypocenter and final hypocenter are displayed in Figures S13 and S12. The mean change in epicenter is about 5 km and the standard deviation of depth changes is about 5.95 km.

In general, after relocation the diffuse seismicity remains diffuse (Figure 13). Similar results were obtained for relocations in the Los Angeles basin by [64]. [64] explained the diffuse hypocenters as a effect of complex 3D brittle structure with interlaced strike-slip faults and thrust faults. The main lineament in our study region, within the Beluga region, is rotated toward a N-S alignment after relocation (Figure 13). Future efforts using new stations and waveform cross-correlation measurements could improve our results.

5. Discussion

Here we summarize our seismological results in the context of previous work within the three regions of interest (Table 1). We then discuss implications for active faults and larger earthquakes in the region.

5.1. Structures and active tectonics in the Cook Inlet and Susitna region

Beluga region

The Beluga region (Figure 12a) is physiographically marked by a triangular-shaped feature which we describe as the Beluga “interlowland region” (BILR), after [69]. The BILR comprises four small mountains, each on the order of 1000 m elevation: Mount Susitna, Little Mount Susitna, unnamed (south of Wolf Lakes), and Beluga Mountain. The BILR is bounded to the northeast by the Susitna basin and the Beluga Mountain fault, to the south by Castle Mountain fault and the Cook Inlet basin, and to the west by a north-south physiographic low that is the drainage for the Talachulitna river, which flows north.

The Beluga region (Figure 12a) contains a seismic lineament named the Talachulitna seismic zone (TSZ) by [38]. The TSZ is approximately aligned with the western margin of the BILR, near the Talachulitna river. [38] interpreted the TSZ to be dipping steeply to the northeast (their Fig. 4c). The scatter in their results—and ours (Figure 12a)—prevents us from identifying any alignment with depth.

Earthquake mechanisms are challenging to estimate for the TSZ. [38] tabulated one focal mechanism in this zone (AF2; their Table 2), from the AEC focal mechanism catalog, but the current AEC catalog

272 has only five events (Figure 11b), none of which pre-date 2005. We present moment tensors for 9 events,
273 all of which are shallower than 12 km (Table S2). The mechanisms have considerable variation, with a
274 predominance of thrust faulting consistent with east-west compression (Figure 12a).

275 Regional geophysical data and geological data provide context for the active seismicity. The BILR is
276 mainly composed of Cenozoic and Mesozoic intrusive rocks [70, 71] that are adjacent to Cenozoic sedimentary
277 basins to the north (Susitna), west (Beluga), and south (Cook Inlet) (Figure 1b). [72, 69] used gravity data
278 and magnetic data to identify the Beluga Mountain fault on the northern front of the BILR as a thrust fault
279 dipping southwest; however recent fault kinematic data do not support a thrust interpretation [73]. The
280 Beluga Mountain fault does not appear to be seismically active or connected with the Talachulitna seismic
281 zone.

282 Examining Figure 12a, we speculate that the Talachulitna seismic zone represents a north-striking, east-
283 dipping thrust fault system that may represent some weakness within the crustal block north of the Castle
284 Mountain fault and west of Susitna basin. This weakness, aligned with the western margin of the BILR,
285 could accommodate some regional compression and contribute to uplift of the BILR.

286 *Upper Cook Inlet region*

287 Earthquakes in the Upper Cook Inlet region occur beneath Cook Inlet basin, a large, long-lived forearc
288 sedimentary basin whose Tertiary strata have a maximal thickness of 7.6 km and overlie a Mesozoic section
289 of approximately 8 km [74, 75, 76]. It is bounded by Aleutian Range to west, Alaska Range and Talkeetna
290 Mountains to the north, Kenai and Chugach Mountains to the east (see Figure 1). Castle Mountain Fault
291 to the north, separates the Cook Inlet basin from the adjoining Susitna basin. The similarities in structures
292 of Cook Inlet and Susitna basins suggests that their histories are linked [76].

293 The 22 events in our study (Figure 12b, Table S3) mostly have depths in the 10–20 km range, placing
294 them either within the Mesozoic strata or the crystalline basement. The crust within Upper Cook Inlet
295 (north of West Foreland) is more seismically active than the Lower Cook Inlet; this is possibly related to
296 the underlying subduction of the Yakutat microplate [4, 77].

297 Folds in Cook Inlet are complex, discontinuous structures with variable shape and vergence that probably
298 developed by right-transpressional deformation on oblique-slip faults extending downward into the Mesozoic
299 strata beneath the Tertiary basin [78]. A discussion of the complex folding and faulting structures in the
300 basin can be found in [74, 79].

301 Our moment tensor inversions for 22 reveals thrust fault mechanisms whose strike angles are generally
302 aligned with the Cook Inlet anticlines [78, 22] (Figure 12b). The simplest explanation is that the anticline
303 structures, identified within active-source seismic data, arise from NW–SE thrust faulting identified from
304 modern earthquakes.

305 *Susitna region*

306 The Susitna region exhibits diffuse seismicity with the larger earthquakes (22 in this study) exhibiting
307 thrust fault mechanisms (Figure 12c, Table S4). These mechanisms, with NW–SE P-axes, are consistent
308 with the convergence direction of N21W [2] between the Pacific and North America plates. They are also
309 consistent with the interpretation of subsurface compressional structures in the region [69].

310 The earthquakes in the Susitna region are within a tectonically complicated region. The region is marked
311 by the Susitna basin (Figure 3b) [80, 81], which is bounded by the Alaska Range to the north, the Talkeetna
312 Mountains to the east, the BILR (and Beluga Mountain fault) to the west, and the Castle Mountain fault to
313 the south. The crustal earthquakes are vertically bounded by the overlying Susitna basin and the underlying
314 subducting Pacific plate. The Pacific plate exhibits two transitions in this region: (1) a kink in its geometry
315 (e.g., Figure 6), from western dipping to more northwestern dipping [8] and (2) an interpreted transition
316 from normal subducting crust in the west to overthickened Pacific/Yakutat crust in the east (Figure 1a). It
317 is possible that either of these slab-related features contributes to the concentration of crustal seismicity in
318 the eastern part of the Susitna region.

319 Comparison between the crustal earthquakes and the basement surface (Figure S11c) reveals several
320 earthquakes below the deepest part of Susitna basin and within the uppermost 10 km. It is possible that
321 these earthquakes occur on deeper extensions of the structures mapped within the subsurface basin structures
322 [28, 18]. The diffuse seismicity in the eastern portion of the Susitna region underlies the shallowest portion
323 of the basin and are not associated with any previously identified subsurface structures.

324 *5.2. Implications of minor earthquakes for active faults*

325 From our perspective, seismic evidence for an active fault includes: (1) alignment of seismicity into a
326 lineament (2) occurrence of moment tensors with one of its two possible fault plane parallel to lineament
327 (3) occurrence of large ($M \geq 6$) earthquakes. This seismic evidence should be assessed alongside geological
328 evidence, whether in the form of slip rates inferred from dated offset units at the surface, from structural
329 offsets inferred from seismic imaging and potential field data, and from paleoseismic evidence of past large
330 earthquakes [23, 22, 69, 21].

331 Our presentation in Figure 12 displays these three types of seismic evidence: relocated hypocenters of
332 modern earthquakes, source mechanisms for the largest modern earthquakes, and estimated epicenters of
333 the largest two historical earthquakes, in 1933 and 1943. We also superimpose previously published faults,
334 and here we discuss the possible connections between faults identified from surface and subsurface geological
335 data with seismic activity at depth.

336 Most of the relocated seismicity does not exhibit seismic lineaments (Section 4). The only lineament
337 we are confident about is the previously identified Talachulitna seismic zone (Figure 12a). It is possible
338 that this seismic zone is an expression of a single fault, but the source mechanisms are variable, and the

339 structure does not have definitive evidence for hosting any moderate or large earthquake. To the northeast,
340 within the Susitna region (Figure 12c), the seismicity is diffuse but the mechanisms are more consistent,
341 exhibiting thrust faulting. Deformation within the crust appears to be broadly distributed, rather than
342 concentrating on a few discrete faults. The same pattern is true to the south, within the Upper Cook
343 Inlet region (Figure 12c): diffuse seismicity with consistent thrust fault mechanisms. In both the Susitna
344 region and the Upper Cook Inlet region, there are subsurface fault and fold structures identified from
345 modeling seismic reflection data and potential field data (gravity, magnetics). If these shallowly-identified
346 faults penetrate below the sedimentary basements (Figure 3b), then it seems reasonable to ascribe the style
347 of faulting inferred from the earthquake mechanisms to the style of faulting occurring near the surface.
348 Therefore we would ascribe thrust faulting to the active folds in Cook Inlet basin [27] and thrust faulting to
349 the structures in Susitna basin [28, 18]. This is in contrast to existing catalog of earthquake mechanisms,
350 which favors strike-slip faulting in these regions (Figure 11).

351 *5.3. Structures responsible for 1933, 1943, and 1954 earthquakes*

352 Large earthquakes rupture along faults with dimensions of tens of kilometers. Previous studies of large
353 sets of earthquakes provides scaling between magnitude and fault dimensions. Assuming a circular fault
354 (radius r , fault dimension $2r$) and a stress drop between 0.2 MPa and 20 MPa [82], the corresponding fault
355 dimension would be

- 356 • 10–44 km for the 1954 M_w 6.4 earthquake
357 • 15–70 km for the 1933 M_w 6.8 earthquake
358 • 27–125 km for the 1943 M_w 7.3 earthquake

359 The empirical relationships of [83] are also within these ranges. These dimensions should be kept in mind
360 when examining Figures 6 and 12.

361 Our probabilistic hypocentral estimations for the 1933, 1943, and 1954 earthquakes (Figure 6, Section 2.1) provide a starting point for interpreting the structures responsible (and not responsible) for these
362 earthquakes. The 1933 earthquake (Figure 6) occurred within the region of the concentration of modern
363 earthquakes in the Upper Cook Inlet region (Figure 12b). It seems possible that one of the northeast-striking
364 thrust faults could have hosted the 1933 earthquake. The 1943 earthquake (Figure 6) maximum likelihood
365 epicenter is on the Beluga Mountain fault (Figure 12c), yet the uncertainty in the epicenter also covers the
366 north-striking faults in Susitna basin, as well as the Talachulitna seismic zone (Figure 12a).

368 Reliable source mechanisms for historical earthquakes would provide valuable constraints on the (un-
369 known) host faults. Here we summarize results, and challenges, from [24], who estimated source mechanisms
370 for the 1933, 1943, and 1954 earthquakes, among others. They used limited teleseismic data to estimate

371 the source mechanisms: P, PP, and S waveforms for 13 global stations, as well as first-motion polarities,
372 where available. (By comparison, there are >100 global stations providing arrival times used in Figures 6
373 and 5.) They present waveform comparisons for all events in their Figure A2, offering the reader the chance
374 to assess the reliability of the results. The numbers of stations and waveforms used for each event were
375 as follows: 3 stations (8 waveforms) for 1933, 5 stations (9 waveforms) for 1943, 6 stations (11 waveforms)
376 plus first-motion polarities for 1954. Surface waves were not used, though they provide stable constraints
377 for global moment tensor inversions [25, 84], mainly owing to the insensitivity of their long periods to 3D
378 structural heterogeneities in Earth.

379 The picture of faulting from the 1933 and 1943 mechanisms [24] is one of strike-slip faulting (Figure 6),
380 either right-lateral on a northeast-striking fault or left-lateral on a northwest-striking fault. Based on the
381 points above, and from our own experience examining moment tensor uncertainties with modern regional
382 earthquakes [48], we would advise caution in basing any interpretation on the historical mechanisms. For
383 example, rotation of these beachballs by 90° about their P-axes would lead to a north-striking thrust fault
384 that would satisfy some of the historical seismic waveforms and first-motion polarities.

385 The Castle Mountain fault—the principal active fault within the Cook Inlet and Susitna region—was not
386 responsible for the 1933 or 1943 earthquakes (Figure 6), corroborating [24]. Two modern earthquakes, each
387 well-recorded by regional stations, provide support for the Castle Mountain fault—or at least the eastern
388 portion—as a right-lateral strike-slip fault. These earthquakes occurred just east of the Cook Inlet and
389 Susitna region, as 1984-08-14 M_w 5.8 (depth 15 km) and 1996-11-11 M_l 4.6 (depth 17 km). A detailed study
390 of the 1984 earthquake was presented in [85].

391 The 1954 earthquake likely occurred within the subducting Pacific plate, rather than on the subduction
392 interface or within the lower overriding crust. The depth distribution of modern seismicity in this region is
393 nearly continuous (Figure 7c, Figure 1b), making it challenging to discriminate among the three possibilities.
394 This event has the benefit of better data than the older events, and therefore the mechanism should be more
395 reliable. Two source mechanisms from previous studies are shown in Figure 6 and reveal strike-slip faulting,
396 not low-angle thrust faulting that would be expected for the subduction interface.

397 6. Summary

398 We present a seismological study of the tectonically complex region of Cook Inlet and Susitna, west of
399 Anchorage, Alaska (Figure 1), with emphasis on crustal earthquakes. Using arrival time data, we estimate
400 hypocenters of all 11 historical earthquakes $M_w \geq 5.8$ that have occurred in the Cook Inlet and Susitna
401 region. Using waveforms from modern earthquakes, we estimate source mechanisms for 53 crustal earth-
402 quakes (M_w 2.5 to 4.8). Using arrival time data, we relocate a catalog of 5726 earthquakes ($M_l \geq 1.5$). We
403 examine these seismological results in the context of regional tectonics, regional structures (basins, faults,

404 folds), and previously published source mechanisms of older (and larger) earthquakes.

405 Here we summarize our main findings:

- 406 1. Within the Cook Inlet and Susitna region, we can generalize the earthquake patterns into two time
407 periods (Figure 4). In the last several decades there have been small-magnitude thrust events in
408 the crust and larger events in the slab. Prior to 1950 or so there have been large-magnitude crustal
409 earthquakes that were possibly strike-slip.

410 The existence of two crustal earthquakes (1933 M_w 6.8 and 1943 M_w 7.3) motivates our examination of
411 modern crustal earthquakes and geological structures. The crust has not produced notable earthquakes
412 in the recent decades of high-quality seismic data: there are zero crustal earthquakes in the GCMT
413 catalog ([25]: 1976–) within our three focus regions (Figure 8b).

- 414 2. Our source mechanisms favor an interpretation of thrust faulting (Figure 11a) over strike-slip faulting
415 (Figure 11b). Uncertainties in the source mechanisms are considerable, owing to the small magnitudes
416 (which limits the inclusion of surface waves) and the extreme crustal heterogeneity (notably basins:
417 Figure 3b), which was not accounted for in modeling synthetic seismograms.
- 418 3. Seismicity in the Susitna region (Figure 12c, Figure 13) is diffuse [67] and may be related to slab
419 dynamics (Section 5.1).
- 420 4. The 1933 M_w 6.8 earthquake occurred beneath Cook Inlet basin, in a region exhibiting northeast-
421 striking thrust fault source mechanisms (Figure 12b) that are aligned with the strike of active fold
422 anticlines [27]. It is possible that the 1933 earthquake ruptured as a thrust fault, though the previously
423 published source mechanism (using 3 stations) is a strike-slip mechanism.
- 424 5. The 1943 M_w 7.3 Susitna earthquake is the fourth largest earthquake ever to occur in mainland Alaska,
425 following 1964 M_w 9.2 megathrust, 2002 M_w 7.9 Denali fault, and 1979 M_w 7.4 Wrangell. Its hypocenter
426 was beneath the Susitna basin, possibly on a structure associated with the Beluga Mountain fault or
427 the Talachulitna seismic zone (Figure 12a). Moment tensors of crustal events closest to the 1943
428 epicenter exhibit thrust mechanisms, consistent with inferred subsurface structures [28, 69].
- 429 6. The 1954 M_w 6.4 earthquake beneath the Kenai peninsula was likely an intraslab earthquake. It
430 produced the strongest shaking (MMI 8) ever documented on the western Kenai peninsula (Appendix
431 A). The subducting Pacific slab has produced much larger earthquakes, such as the deeper and farther
432 away M_w 7.1 earthquake on 2016-01-24. For scenario earthquakes, it is worth considering a M_w 7.0
433 earthquake in the 1954 hypocentral region.
- 434 7. There appears to be a concentration of active seismicity and also large historical earthquakes (1933,
435 1943) beneath the deepest sedimentary basins (Cook Inlet and Susitna: Figure 3b). It is possible that
436 the dynamical processes that influence basin development—over the past millions of years—are also
437 responsible for modern earthquakes. Alternatively, modern earthquakes could arise from reactivation
438 of ancient faults.

439 **7. Acknowledgments**

440 This project was supported by the Earthquakes Hazards Program of the United States Geological Sur-
441 vey, Award G15AP00052. We thank Domenico Di Giacomo of the International Seismological Centre for
442 providing arrival time data for six of the historical earthquakes presented here and in [43]: 1929-07-03,
443 1933-06-12, 1933-06-13, 1933-06-19, 1936-10-23, 1937-10-24. We thank Celso Alvizuri for code developments
444 for data processing and moment tensor inversions.

445 **References**

- 446 [1] R. A. Page, N. N. Biswas, J. C. Lahr, H. Pulpan, Seismicity of continental Alaska, in: D. B. Slemmons, E. R. Engdahl,
447 M. D. Zoback, D. D. Blackwell (Eds.), Neotectonics of North America, The Geology of North America, Geol. Soc. Am.,
448 Boulder, Colo., USA, 1991, Ch. 4, pp. 47–68, Decade Map Volume 1.
449 [2] P. Bird, An updated digital model of plate boundaries, *Geochem. Geophys. Geosyst.* 4 (2003) 1–52.
450 doi:10.1029/2001GC000252.
451 [3] G. Plafker, T. L. Hudson, T. Bruns, M. Rubin, Late Quaternary offsets along the Fairweather fault and crustal plate
452 interactions in southern Alaska, *Can. J. Earth Sci.* 15 (5) (1978) 805–816.
453 [4] D. Eberhart-Phillips, D. H. Christensen, T. M. Brocher, R. Hansen, N. A. Ruppert, P. J. Haeussler, G. A. Abers, Imaging
454 the transition from Aleutian subduction to Yakutat collision in central Alaska, with local earthquakes and active source
455 data, *J. Geophys. Res.* 111. doi:10.1029/2005JB004240.
456 [5] G. L. Christeson, S. P. S. Gulick, H. J. A. van Avendonk, L. L. Worthington, R. S. Reece, T. L. Pavlis, The Yakutat
457 terrane: Dramatic change in crustal thickness across the Transition fault, Alaska, *Geology* 38 (10) (2010) 895–898.
458 [6] S. Rondenay, L. G. J. Montési, G. A. Abers, New geophysical insight into the origin of the Denali volcanic gap, *Geo-
459 phys. J. Int.* 182 (2010) 613–630.
460 [7] J. Li, G. A. Abers, Y. Kim, D. Christensen, Alaska megathrust 1: Seismicity 43 years after the great 1964 Alaska
461 megathrust earthquake, *J. Geophys. Res.* 118 (2013) 4861–4871. doi:10.1002/jgrb.50358.
462 [8] N. A. Ratchkovski, R. A. Hansen, New evidence for segmentation of the Alaska subduction zone, *Bull. Seis-
463 mol. Soc. Am.* 92 (5) (2002) 1754–1765.
464 [9] J. Davies, L. Sykes, K. Jacob, Shumagin seismic gap, Alaska Peninsula: History of great earthquakes, tectonic setting,
465 and evidence for high seismic potential, *J. Geophys. Res.* 86 (B5) (1981) 3821–3855.
466 [10] G. Ichinose, P. Somerville, H. K. Thio, R. Graves, D. O'Connell, Rupture process of the 1964 Prince William
467 Sound, Alaska, earthquake from the combined inversion of seismic, tsunami, and geodetic data, *J. Geophys. Res.* 112.
468 doi:10.1029/2006JB004728.
469 [11] Y. Ohta, J. T. Freymueller, S. Hreinsdóttir, H. Suito, A large slow slip event and the depth of the seismogenic zone in the
470 south central Alaska subduction zone, *Earth Planet. Sci. Lett.* 247 (2006) 108–116.
471 [12] M. Wei, J. J. McGuire, E. Richardson, A slow slip event in the south central Alaska Subduction Zone and related seismicity
472 anomaly, *Geophys. Res. Lett.* 39. doi:10.1029/2012GL052351.
473 [13] Y. Fu, J. T. Freymueller, Repeated large Slow Slip Events at the south central Alaska subduction zone, *Earth Planet.
474 Sci. Lett.* 375 (2013) 303–311.
475 [14] S. Li, J. Freymueller, R. McCaffrey, Slow slip events and time-dependent variations in locking beneath Lower Cook Inlet
476 of the Alaska-Aleutian subduction zone, *J. Geophys. Res. Solid Earth* 121 (2016) 1060–1079. doi:10.1002/2015JB012491.
477 [15] E. Veenstra, D. H. Christensen, G. A. Abers, A. Ferris, Crustal thickness variation in south-central Alaska, *Geology* 34 (9)
478 (2006) 781–784.

- 479 [16] S. R. Capps, The Yentna District Alaska, Bulletin 534 (1913).
- 480 [17] J. H. Dover, Geologic map and fold- and thrust-belt interpretation of the southeastern part of the Charley River Quad-
- 481 rangle, east-central Alaska, Miscellaneous Investigations Series Map 1942, 14 p., 2 sheets, scale 1:100,000 (1992).
- 482 [18] P. J. Haeussler, R. W. Saltus, R. G. Stanley, N. Ruppert, K. Lewis, S. M. Karl, A. Bender, The Peters Hills basin, a
- 483 Neogene wedge-top basin on the Broad Pass thrust fault, south-central Alaska, *Geosphere* 1464–1488.
- 484 [19] A. Grantz, Strike-Slip Faults in Alaska, 1966, U.S. Geol. Survey Open-File Report 66-53, Washngton, D.C.
- 485 [20] J. B. Willis, P. J. Haeussler, R. L. Bruhn, G. C. Willis, Holocene slip rate for the western segment of the castle mountain
- 486 fault, alaska, *Bulletin of the Seismological Society of America* 97 (3) (2007) 1019–1024. doi:10.1785/0120060109.
- 487 [21] R. D. Koehler, G. A. Carver.
- 488 [22] R. D. Koehler, R.-E. Farrell, P. A. C. Burns, R. A. Combelick, Quaternary faults and folds in Alaska: A digital
- 489 database, Alaska Div. Geol. Geophys. Surv. Miscellaneous Publication 141, 31 p., 1 sheet, scale 1:3,700,000 (2012).
- 490 doi:10.14509/23944.
- 491 [23] P. J. Haeussler, T. C. Best, C. F. Waythomas, Paleoseismology at high latitudes: Seismic disturbance of upper Quaternary
- 492 depositis along the Castle Mountain fault near Houston, Alaska, *Geol. Soc. Am.* 114 (10) (2002) 1296–1310.
- 493 [24] D. I. Doser, W. A. Brown, A study of historic earthquakes of the Prince William Sound, Alaska, Region, *Bull. Seis-*
- 494 *mol. Soc. Am.* 91 (4) (2001) 842–857.
- 495 [25] A. Dziewonski, T.-A. Chou, J. H. Woodhouse, Determination of earthquake source parameters from waveform data for
- 496 studies of global and regional seismicity, *J. Geophys. Res.* 86 (B4) (1981) 2825–2852. doi:10.1029/JB086iB04p02825.
- 497 [26] G. Ekström, M. Nettles, A. M. Dziewoński, The global GCMT project 2004–2010: Centroid-moment tensors for 13,017
- 498 earthquakes, *Phys. Earth Planet. Inter.* 200–201 (2012) 1–9. doi:10.1016/j.pepi.2012.04.002.
- 499 [27] R. L. Bruhn, P. J. Haeussler, Deformation driven by subduction and microplate collision: Geodynamics of Cook Inlet
- 500 basin, Alaska, *Geol. Soc. Am. Bull.* 118 (3/4) (2006) 289–303.
- 501 [28] K. A. Lewis, C. J. Potter, A. K. Shah, R. G. Stanley, P. J. Haeussler, R. W. Saltus, Preliminary Interpretation of Industry
- 502 Two-Dimensional Seismic Data from Susitna Basin, South-Central Alaska, U.S. Geol. Survey open-file report 2015-1138
- 503 (2015). doi:10.3133/ofr20151138.
- 504 [29] B. Gutenberg, C. F. Richter, *Seismicity of the Earth and Associated Phenomena*, 2nd Edition, Princeton U. Press,
- 505 Princeton, New Jersey, USA, 1954.
- 506 [30] F. Waldhauser, W. L. Ellsworth, A double-difference earthquake location algorithm: Method and application to the
- 507 Northern Hayward fault, California, *Bull. Seismol. Soc. Am.* 90 (6) (2000) 1353–1368. doi:10.1785/0120000006.
- 508 [31] D. A. Storchak, D. Di Giacomo, I. Bondár, E. R. Engdahl, J. Harris, W. H. K. Lee, A. Villaseñor, P. Bormann, Public
- 509 release of the ISC–GEM Global Instrumental Earthquake Catalogue (1900–2009), *Seismol. Res. Lett.* 84 (5) (2013) 810–815.
- 510 doi:10.1785/0220130034.
- 511 [32] International Seismological Centre, ISC-GEM Global Instrumental Earthquake Catalogue, Version 5.0, released on 2018-
- 512 02-27 (2018).
- 513 [33] E. R. Engdahl, R. van der Hilst, R. Buland, Global teleseismic earthquake relocation with improved travel times and
- 514 procedures for depth determination, *Bull. Seismol. Soc. Am.* 88 (3) (1998) 722–743.
- 515 [34] I. Bondár, D. Storchak, Improved location procedures at the International Seismological Centre, *Geophys. J. Int.* 186 (2011)
- 516 1220–1244. doi:10.1111/j.1365-246X.2011.05107.x.
- 517 [35] D. D. Giacomo, I. Bondár, D. A. Storchak, E. R. Engdahl, P. Bormann, J. Harris, ISC-GEM: Global instrumental earth-
- 518 quake catalogue (1900–2009), III. re-computed MS and mb, proxy MW, final magnitude composition and completeness
- 519 assessment, *Physics of the Earth and Planetary Interiors* 239 (2015) 33–47. doi:10.1016/j.pepi.2014.06.005.
- 520 [36] D. I. Doser, Relocations of earthquakes (1899–1917) in south-central alaska, *Pure and Applied Geophysics* 163 (8) (2006)
- 521 1461–1476. doi:10.1007/s00024-006-0085-3.

- 522 [37] D. I. Doser, Historical seismicity (1918–1964) of the Kodiak Island region, Bull. Seismol. Soc. Am. 95 (3) (2005) 878–895.
 523 doi:10.1785/0120040175.
- 524 [38] C. Flores, D. I. Doser, Shallow seismicity of the Anchorage, Alaska, Region (1964–1999), Bull. Seismol. Soc. Am. 95 (5)
 525 (2005) 1865–1879. doi:10.1785/0120040121.
- 526 [39] A. Lomax, J. Virieux, P. Volant, C. Berge, Probabilistic earthquake location in 3D and layered models: Introduction of
 527 a Metropolis-Gibbs method and comparison with linear locations, in: C. H. Thurber, N. Rabinowitz (Eds.), Advances in
 528 Seismic Event Location, Kluwer, Amsterdam, 2000, pp. 101–134.
- 529 [40] B. L. N. Kennett, E. R. Engdahl, R. Buland, Constraints on seismic velocities in the Earth from traveltimes, Geophys. J. Int. 122 (1995) 108–124.
- 531 [41] H. P. Crotwell, T. J. Owens, J. Ritsema, The TauP Toolkit: Flexible Seismic travel-time and ray-path utilities, Seismol. Res. Lett. 70 (2) (1999) 154–160.
- 533 [42] International Seismological Centre, On-line Bulletin, <http://www.isc.ac.uk>, Internat'l. Seis. Cent., Thatcham, United Kingdom (accessed 2017-05-03) (2015).
- 535 [43] A. Lomax, V. Silwal, C. Tape, Hypocenter estimation for 14 earthquakes in south-central Alaska (1929–1975), Scholar-
 536 Works@UA at <http://hdl.handle.net/11122/8380>: descriptor file and zipped set of text files for each earthquake (2018).
- 537 [44] S. R. Brockman, A. F. Espinosa, J. A. Michael, Catalog of Intensities and Magnitudes for Earthquakes in Alaska and the
 538 Aleutian Islands—1786–1981, 1988, U.S. Geol. Survey Bulletin 1840.
- 539 [45] G. Abers, D. Christensen, Seismic and geodetic imaging of subducting terranes under North America, International
 540 Federation of Digital Seismograph Networks. Other/Seismic Network. doi:10.7914/SN/YV_2006 (2006).
- 541 [46] C. Tape, D. Christensen, M. M. Moore-Driskell, J. Sweet, K. Smith, Southern Alaska Lithosphere and Mantle Observ-
 542 ation Network (SALMON): a seismic experiment covering the active arc by road, boat, plane, and helicopter, Seismol. Res. Lett. 88 (4) (2017) 1185–1202. doi:10.1785/0220160229.
- 544 [47] C. Tape, D. H. Christensen, M. M. Driskell, Southern Alaska Lithosphere and Mantle Observation Network, International
 545 Federation of Digital Seismograph Networks. Other/Seismic Network. doi:10.7914/SN/ZE_2015 (2015).
- 546 [48] V. Silwal, C. Tape, Seismic moment tensors and estimated uncertainties in southern Alaska, J. Geophys. Res. Solid
 547 Earth 121 (2016) 2772–2797. doi:10.1002/2015JB012588.
- 548 [49] L.-S. Zhao, D. V. Helmberger, Source estimation from broadband regional seismograms, Bull. Seismol. Soc. Am. 84 (1)
 549 (1994) 91–104.
- 550 [50] L. Zhu, D. Helmberger, Advancement in source estimation techniques using broadband regional seismograms, Bull. Seis-
 551 mol. Soc. Am. 86 (5) (1996) 1634–1641.
- 552 [51] L. Zhu, L. A. Rivera, A note on the dynamic and static displacements from a point source in multilayered media,
 553 Geophys. J. Int. 148 (2002) 619–627. doi:10.1046/j.1365-246X.2002.01610.x.
- 554 [52] C. Alvizuri, C. Tape, Full moment tensors for small events ($M_w < 3$) at Uturuncu volcano, Bolivia, Geophys. J. Int. 206
 555 (2016) 1761–1783. doi:10.1093/gji/ggw247.
- 556 [53] C. Alvizuri, V. Silwal, L. Krischer, C. Tape, Estimation of full moment tensors, including uncertainties, for nuclear
 557 explosions, volcanic events, and earthquakes, J. Geophys. Res. Solid Earth (in press) doi:10.1029/2017JB015325.
- 558 [54] S. R. Ford, W. R. Walter, D. S. Dreger, Event discrimination using regional moment tensors with teleseismic- P constraints,
 559 Bull. Seismol. Soc. Am. 102 (2) (2012) 867–872. doi:10.1785/0120110227.
- 560 [55] A. Guilhem, L. Hutchings, D. S. Dreger, L. R. Johnson, Moment tensor inversions of $M \sim 3$ earthquakes in the Geysers
 561 geothermal fields, California, J. Geophys. Res. Solid Earth 119 (3) (2014) 2121–2137. doi:10.1002/2013JB010271.
- 562 [56] A. Chiang, D. S. Dreger, S. R. Ford, W. R. Walter, Source characterization of underground explosions from combined re-
 563 gional moment tensor and first-motion analysis, Bull. Seismol. Soc. Am. 104 (4) (2014) 1587–1600. doi:10.1785/0120130228.
- 564 [57] Z. Wéber, Probabilistic joint inversion of waveforms and polarity data for double-couple focal mechanisms of local earth-

- 565 quakes, *Geophys. J. Int.*213 (2018) 1586–1598. doi:10.1093/gji/ggy096.
- 566 [58] S. C. Stähler, K. Sigloch, Fully probabilistic seismic source inversion – Part 2: Modelling errors and station covariances, *Solid Earth*7 (2016) 1521–1536. doi:10.5194/se-2016-87.
- 567 [59] M. Mustać, H. Tkalčić, Point source moment tensor inversion through a Bayesian hierarchical model, *Geophys. J. Int.*204 (2016) 311–323. doi:10.1093/gji/ggv458.
- 568 [60] M. Mustać, H. Tkalčić, On the use of data noise as a site-specific weight parameter in a hierarchical Bayesian moment tensor inversion: The case study of The Geysers and Long Valley caldera earthquakes, *Bull. Seismol. Soc. Am.*107 (4) (2017) 1914–1922. doi:10.1785/0120160379.
- 569 [61] C. Alvizuri, C. Tape, Full moment tensor analysis of nuclear explosions in North Korea, *Seismol. Res. Lett.* (submitted).
- 570 [62] V. Silwal, Seismic moment tensor catalog for crustal earthquakes in the Cook Inlet and Susitna region of southern Alaska, ScholarWorks@UA at <http://hdl.handle.net/11122/8383>: descriptor file, text file of catalog, figures with waveform fits, and input weight files (2018).
- 571 [63] P. Reasenberg, D. Oppenheimer, FPFIT, FPPLT and FPPAGE: Fortran computer programs for calculating and displaying earthquake fault-plane solutions, Open-File Report 85-739 (1985).
- 572 [64] E. Hauksson, P. Shearer, Southern California hypocenter relocation with waveform cross-correlation, Part 1: Results using the double-difference method, *Bull. Seismol. Soc. Am.*95 (3) (2005) 896–903.
- 573 [65] P. Shearer, E. Hauksson, G. Lin, Southern California hypocenter relocation with waveform cross-correlation, Part 2: Results using source-specific station terms and cluster analysis, *Bull. Seismol. Soc. Am.*95 (3) (2005) 904–915. doi:10.1785/0120040168.
- 574 [66] H. Zhang, C. H. Thurber, Double-difference tomography: the method and its application to the Hayward fault, California, *Bull. Seismol. Soc. Am.*93 (5) (2003) 1875–1889. doi:10.1785/0120020190.
- 575 [67] N. A. Ratchkovsky, J. Pujol, N. N. Biswas, Relocation of shallow earthquakes in southern Alaska using Joint Hypocenter Determination method, *J. Seis.*2 (1998) 87–102.
- 576 [68] A. Douglas, Joint epicentre determination, *Nature*215 (1967) 47–48.
- 577 [69] R. W. Saltus, R. G. Stanley, P. J. Haeussler, J. V. Jones III, C. J. Potter, K. A. Lewis, Late Oligocene to present contractional structure in and around the Susitna basin, Alaska—Geophysical evidence and geological implications, *Geosphere*12 (5) (2016) 1–13. doi:10.1130/GES01279.1.
- 578 [70] K. D. Ridgway, J. M. Trop, E. S. Finzel, Modification of continental forearc basins by flat-slab subduction processes: A case study from southern Alaska, in: C. Busby, A. A. Perez (Eds.), *Tectonics of Sedimentary Basins: Recent Advances*, Wiley-Blackwell, 2012, pp. 327–346. doi:10.1002/9781444347166.ch16.
- 579 [71] D. L. LePain, R. G. Stanley, N. T. Harun, K. P. Helmold, R. M. Tsigonis, Reconnaissance stratigraphic studies in the Susitna basin, Alaska, during the 2014 field season, Preliminary Interpretive Report 2015-3-2 (2015). doi:10.14509/29466.
- 580 [72] S. W. Hackett, Gravity survey of Beluga Basin and adjacent area, Cook Inlet region, southcentral Alaska (1977). doi:10.14509/377.
- 581 [73] R. J. Gillis, T. M. Herriott, R. M. Tsigonis, Preliminary results of reconnaissance structural studies of the western Susitna basin, south-central Alaska, Preliminary Interpretive Report 2015-3-5 (2015). doi:10.14509/29469.
- 582 [74] M. A. Fisher, L. B. Magoon, Geologic framework of lower Cook Inlet, *Am. Assoc. Petroleum Geol. Bull.*62 (3) (1978) 373–402.
- 583 [75] D. P. Shellenbaum, L. S. Gregersen, P. R. Delaney, Top Mesozoic unconformity depth map of the Cook Inlet Basin, Alaska, Alaska Div. Geol. Geophys. Surv. Report of Investigation 2010-2, 1 sheet, scale 1:500,000, available at <http://www.dggs.alaska.gov/pubs/id/21961> (last accessed 2016-10-30) (2010). doi:10.14509/21961.
- 584 [76] D. L. LePain, R. G. Stanley, K. P. Helmold, D. P. Shellenbaum, *Geologic Framework and Petroleum Systems of Cook Inlet Basin, South-Central Alaska*, Vol. 104, American Association of Petroleum Geologists, 2013.

- 608 doi:10.1306/13491874M1043621.
- 609 [77] P. J. Haeussler, An overview of the neotectonics of interior Alaska: Far-field deformation from the Yakutat microplate
610 collision, in: J. T. Freymueller, P. J. Haeussler, R. Wesson, G. Ekström (Eds.), Active Tectonics and Seismic Potential of
611 Alaska, Vol. 179 of Geophysical Monograph, Am. Geophys. Un., Washington, D.C., 2008, pp. 83–108.
- 612 [78] P. J. Haeussler, R. L. Bruhn, T. L. Pratt, Potential seismic hazards and tectonics of the upper Cook Inlet basin, Alaska,
613 based on analysis of Pliocene and younger deformation, *Geol. Soc. Am. Bull.* 112 (9) (2000) 1414–1429.
- 614 [79] P. J. Haeussler, R. W. Saltus, Location and extent of Tertiary structures in Cook Inlet basin, Alaska, and mantle dynamics
615 that focus deformation and subsidence, in: J. A. Dumoulin, J. P. Galloway (Eds.), Studies by the U.S. Geological Survey
616 in Alaska 2008–2009, U.S. Geol. Survey, Washington, D.C., 2011, pp. 1–26, Professional Paper 1776-D.
- 617 [80] C. E. Kirschner, Map Showing Sedimentary Basins of Onshore and Continental Shelf Areas, Alaska, U.S. Geol. Survey
618 Miscellaneous Investigation Series I-1873 (1988).
- 619 [81] F. H. Wilson, C. P. Hults, H. R. Schmoll, P. J. Haeussler, J. M. Schmidt, L. A. Yehle, K. A. Labay, Preliminary Geologic
620 Map of the Cook Inlet Region, Alaska, Open-File Report 2009-1108 (2009).
- 621 [82] P. M. Shearer, G. A. Prieto, E. Hauksson, Comprehensive analysis of earthquake source spectra in southern California,
622 *J. Geophys. Res.* 111. doi:10.1029/2005JB003979.
- 623 [83] P. M. Mai, G. C. Beroza, Source scaling properties from finite-fault-rupture models, *Bull. Seismol. Soc. Am.* 90 (3) (2000)
624 604–615.
- 625 [84] Z. Duputel, L. Rivera, H. Kanamori, G. Hayes, W phase source inversion for moderate to large earthquakes, *Geo-
626 phys. J. Int.* 189 (2012) 1125–1147.
- 627 [85] J. C. Lahr, P. A. Page, C. D. Stephens, K. A. Fogelman, Sutton, Alaska, earthquake of 1984: Evidence for activity on
628 the Talkeetna segment of the Castle Mountain fault system, *Bull. Seismol. Soc. Am.* 76 (4) (1986) 967–983.
- 629 [86] K. Abe, Magnitudes of large shallow earthquakes from 1904 to 1980, *Phys. Earth Planet. Inter.* 27 (1981) 72–92.
- 630 [87] E. R. Engdahl, A. Villaseñor, Global seismicity: 1900–1999, in: W. H. K. Lee, H. Kanamori, P. C. Jennings, C. Kisslinger
631 (Eds.), International Handbook of Earthquake and Engineering Seismology, Vol. 81A of International Geophysics Series,
632 Academic Press, London, 2002, pp. 665–690.
- 633 [88] M. A. Jadamec, M. I. Billen, Reconciling surface plate motions with rapid three-dimensional mantle flow around a slab
634 edge, *Nature* 465 (2010) 338–342. doi:10.1038/nature09053.
- 635 [89] G. P. Hayes, D. J. Wald, R. L. Johnson, Slab1.0: A three-dimensional model of global subduction zone geometries,
636 *J. Geophys. Res.* 117. doi:10.1029/2011JB008524.
- 637 [90] Y. Wang, C. Tape, Seismic velocity structure and anisotropy of the Alaska subduction zone derived from surface wave
638 tomography, *J. Geophys. Res. Solid Earth* 119 (2014) 8845–8865. doi:10.1002/2014JB011438.
- 639 [91] C. Amante, B. W. Eakins, ETOPO1 1 Arc-Minute Global Relief Model: Procedures, Data Sources and Analysis, NOAA
640 Technical Memorandum NESDIS NGDC-24, 19 pp. (2009).
- 641 [92] R. G. Stanley, P. J. Haeussler, J. A. Benowitz, D. K. Goodman, R. L. Ravn, D. P. Shellenbaum, R. W. Saltus, K. A.
642 Lewis, C. J. Potter, New stratigraphic revelations in the subsurface susitna basin, south-central alaska, from geochronology
643 and biostratigraphy [poster]: GSA cordilleran section meeting, fresno, CA, may 22, 2013, Tech. rep., Alaska Division of
644 Geological & Geophysical Surveys (May 2013). doi:10.14509/26887.
- 645 [93] J. G. Meyer Jr., Principal facts for gravity data collected in the northern Susitna Basin area, southcentral Alaska, Alaska
646 Alaska Div. Geol. Geophys. Surv. Preliminary Interpretive Report 2005-5 (2005).
- 647 [94] A. J. Wickens, J. H. Hodgson, Computer Re-Evaluation of Earthquake Mechanism Solutions, Publications of the Dominion
648 Observatory, Vol. 33, No. 1, Ottawa, Canada Department of Energy, Mines, and Resources, Contribution 103 to the
649 International Upper Mantle Project (1967).
- 650 [95] F. Neumann, United States Earthquakes 1933, U.S. Department of Commerce, 1935.

651 [96] R. R. Bodle, United States Earthquakes 1943, U.S. Department of Commerce, 1945.

652 [97] L. M. Murphy, W. K. Cloud, United States Earthquakes 1954, U.S. Department of Commerce, 1956.

Table 1: Earthquake selection for three target subregions and for the full region. N_e is the number of earthquakes analyzed in each region for a particular method.

Region	longitude		latitude		method	N_e	max depth (km)	min mag	date range
	min (°)	max (°)	min (°)	max (°)					
Beluga region	-151.50	-151.10	61.25	61.90	moment tensor	9	30	M_l 2.5	2007-08-15 2017-01-01
Upper Cook Inlet region	-151.50	-150.60	60.60	61.25	moment tensor	22	30	M_l 2.5	2007-08-15 2017-01-01
Susitna region	-151.10	-149.90	61.50	62.50	moment tensor	22	30	M_l 3.0	2007-08-15 2017-01-01
Cook Inlet and Susitna region	-151.75	-149.50	60.50	62.50	historical	12	200	M_w 5.8	1904-01-01 2017-01-01
	-152.00	-149.00	60.50	62.50	double difference	5726	30	M_l 1.5	1990-01-01 2017-01-01

Table 2: Earthquakes $M \geq 5.8$ in the Cook Inlet and Susitna region (Table 1) of south-central Alaska since the start of the instrumental era in 1904. The events are selected from the ISC-GEM catalog (before 1976-01-01) and GCMT catalog (after 1976-01-01). ISCG = ISC-GEM 5.0 [31], GCMT = Global Centroid Moment Tensor catalog [25, 26]. NA means that the earthquake was outside the time interval of a particular study.

origin time	ref.	mag. M_w	ref.	GR[29] M	Abe[86] M_s, m_b	EV[87] M_w	DB[24] M_w
1933-04-27 02:36:07	ISCG	6.78	ISCG	7.0	6.9, 7.1	6.90	7.0
1933-06-12 15:23:41	ISCG	5.82	ISCG	–	–	–	–
1933-06-13 22:19:51	ISCG	5.97	ISCG	6.25	–	–	–
1933-06-19 18:47:46	ISCG	5.85	ISCG	6.0	–	–	–
1934-06-18 09:13:52	ISCG	5.97	ISCG	6.75	–	6.60	6.1
1936-10-23 06:24:21	ISCG	6.82	ISCG	–	–	–	–
1941-07-30 01:51:29	ISCG	6.39	ISCG	6.25	–	–	6.3
1943-11-03 14:32:20	ISCG	7.34	ISCG	7.3	7.4, 7.1	7.20	7.0
1954-10-03 11:18:48	ISCG	6.36	ISCG	NA	–	–	6.6
1974-12-29 18:25:01	ISCG	5.92	ISCG	NA	–	–	NA
1975-01-01 03:55:13	ISCG	5.92	ISCG	NA	–	7.40	NA
1991-05-01 07:18:46	GCMT	6.30	GCMT	NA	NA	6.2	NA

Table 3: Estimated depths, with uncertainties, for the earthquakes in Table 2. The depths from NonLinLoc (NLL) are for the maximum likelihood; Figure 7 shows examples of the depth distribution of all posterior hypocenters. The right three columns list the vertical distance from the ISC-GEM epicenter to the subduction interface, for three different interface models. Events marked as * are likely slab events. For the Engdahl catalog, DEQ means that depth is a free parameter, and FEQ means that depth is fixed based on independent information.

	NLL (this study)	GR [29]	DB [24]	EV [87]	ISCG [31]	JB10 [88]	H12 [89]	L13 [7]
1933-04-27	0.33	0	9 ± 4	35 (FEQ)	15 ± 4	54	68	63
1933-06-12	0.65	0	—	—	15 ± 9	71	77	73
1933-06-13	12.71	0	—	—	15 ± 9	85	87	82
1933-06-19	16.29	0	—	—	15 ± 7	64	71	66
1934-06-18*	49.20	80	76 ± 10	50 (DEQ)	60 ± 9	63	72	66
1936-10-23	0.33	—	—	—	15 ± 14	56	68	63
1941-07-30	0.33	0	—	—	35 ± 14	49	64	59
1943-11-03	17.27	0	27 ± 4	35 (FEQ)	15 ± 4	73	75	71
1954-10-03*	55.88	N/A	60 ± 10	64	62 ± 5	40	52	45
1974-12-29*	68.10	N/A	N/A	—	65 ± 5	56	64	57
1975-01-01*	64.03	N/A	N/A	—	63 ± 5	43	57	48
		GCMT	AEC					
1991-05-01*		118	115	114 (DEQ)	113 ± 5	123	110	100

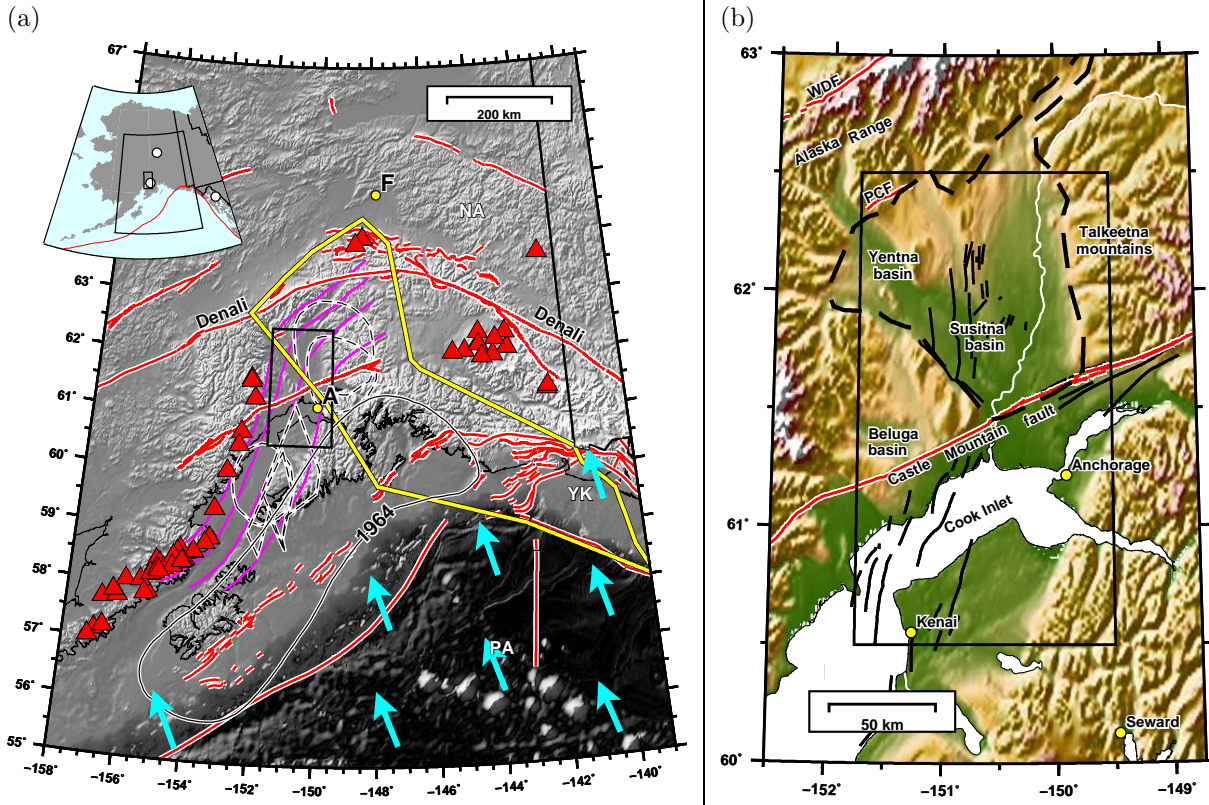
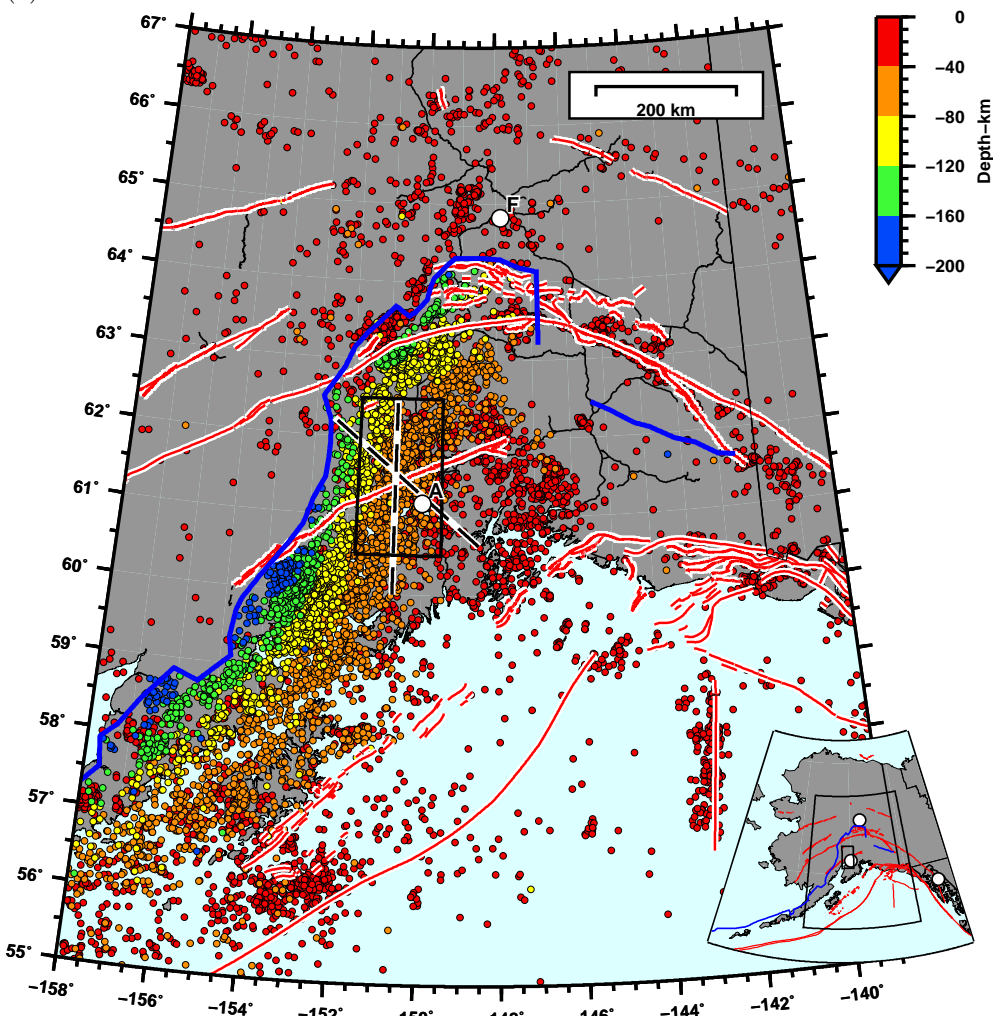


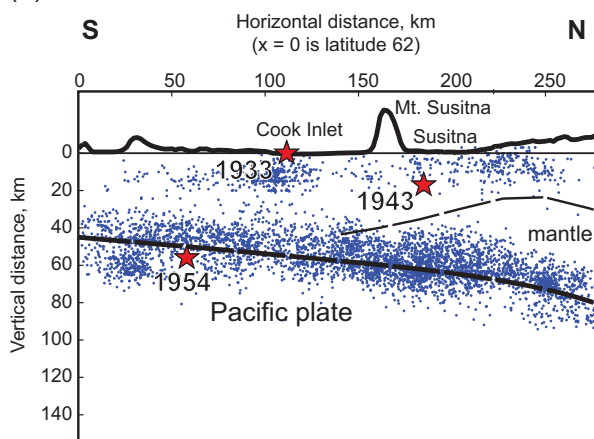
Figure 1: (a) Active tectonic setting of the Aleutian–Alaskan subduction zone, south-central Alaska. The rectangle in the middle shows the main study region. Cyan arrows show the plate vectors for the subducting Pacific plate (PA) under the North American plate (NA) [2]. Magenta curves are the 40 km, 60 km, 80 km, and 100 km contours of the top of the Pacific plate [7]. Yellow bounded region denotes the surface and subsurface extent of the Yakutat block (YK) [4]. Red triangles represent active volcanoes. Black dashed lines are inferred slow-slip from various sources [11, 12, 13, 14]. Also marked is the aftershock zone of the 1964 M_w 9.2 earthquake. Labeled cities: Anchorage (A) and Fairbanks (F). (b) Physiographic map of the Cook Inlet and Susitna region, south-central Alaska. Active faults are plotted in red and include Castle Mountain, Pass Creek (PCF) and the western Denali fault (WDF) at upper left [22]. Other active faults [18] and folds [22] are marked in black. Sedimentary basins are labeled: Cook Inlet, Susitna, Yentna, and Beluga. Cook Inlet basin underlies Cook Inlet and the western Kenai peninsula [75]. Black dashed lines are the boundaries of Susitna basin from [80].

653 Figure 2 [FOLLOWING PAGE]:
654 Seismicity in south-central Alaska. (a) Alaska Earthquake Center (AEC) catalog: $M_w \geq 2$, 1990-01-01 to
655 2017-01-01, colored by depth. The box, containing Anchorage (A), is the focus region of this study; the two
656 profiles are shown in (b) and (c). The red lines are the active faults from [22]. The blue line is the lateral
657 extent of slab seismicity, digitized from the full AEC catalog. (b) S–N cross-section of (a) along the longitude
658 line of -150.75° . Seismicity within 20 km of the profile is shown. Three large earthquakes of interest are
659 projected onto the profile: 1933 $M_w 6.78$, 1943 $M_w 7.34$, and 1954 $M_w 6.36$; the hypocenters are estimated
660 from NonLinLoc. Geometric boundaries shown are the plate interface [7], the Moho [90], and topography
661 [91] exaggerated by a factor of 20. (c) SE–NW cross-section of (a) between Anchorage ($x = 0$ km) and the
662 1943 earthquake.

(a)



(b)



(c)

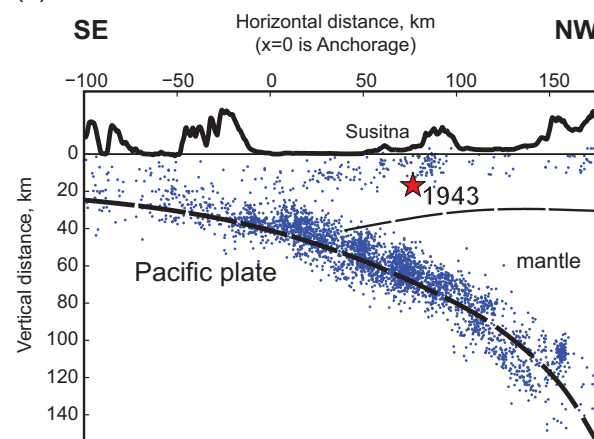


Figure 2:

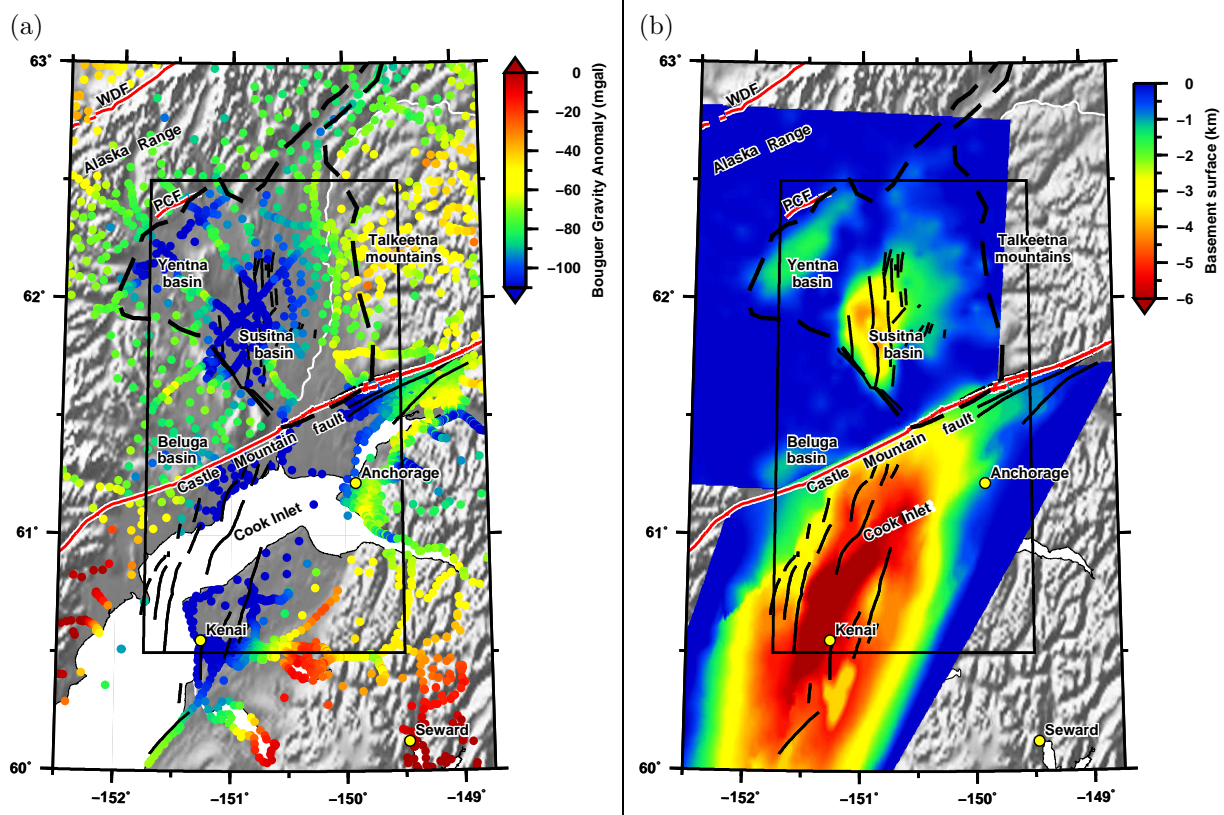


Figure 3: Gravity data and estimated basement depths for the Cook Inlet and Susitna region; see physiographic map in Figure 1b for comparison. Faults and folds plotted include active faults [22], active folds in Cook Inlet [27, 22], and faults in the Susitna basin [28, 18]. (a) Bouguer gravity data [69]. (b) Maps of depth to Tertiary basement for Cook Inlet basin [75], as well as basement surfaces for Susitna basin [81], Yentna basin, and Beluga basin [92]. The dashed outline is the basin-bounding region of [80, 93].

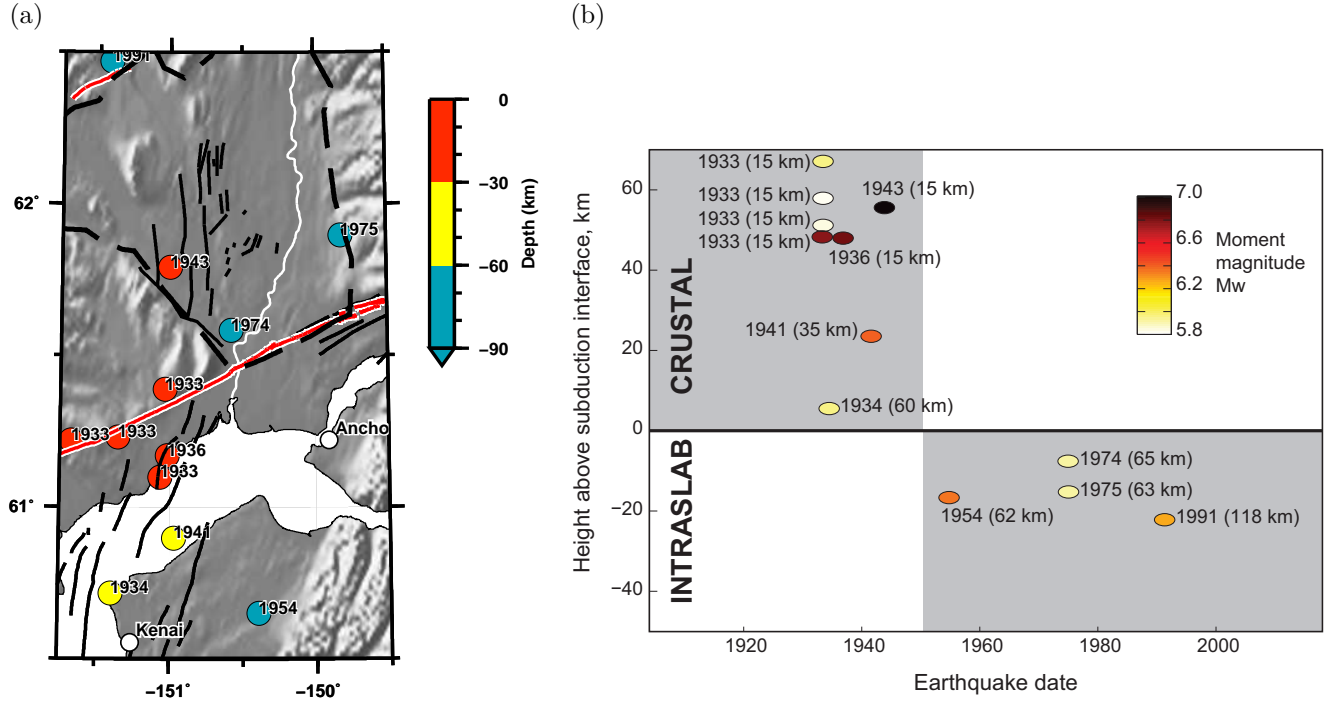


Figure 4: All 12 major earthquakes ($M_w \geq 5.8$) in the Cook Inlet and Susitna region (see Table 1) Earthquakes are selected from the ISC-GEM catalog for the time interval 1904-01-01 to 2017-01-01. (a) Map showing epicenters, colored by depth. (b) Plot of height above subduction interface [7] as a function of origin time, for the 12 earthquakes in (a). The checkered shading at the year of 1950 accentuates the pattern of early crustal earthquakes and later (more recent) slab earthquakes.

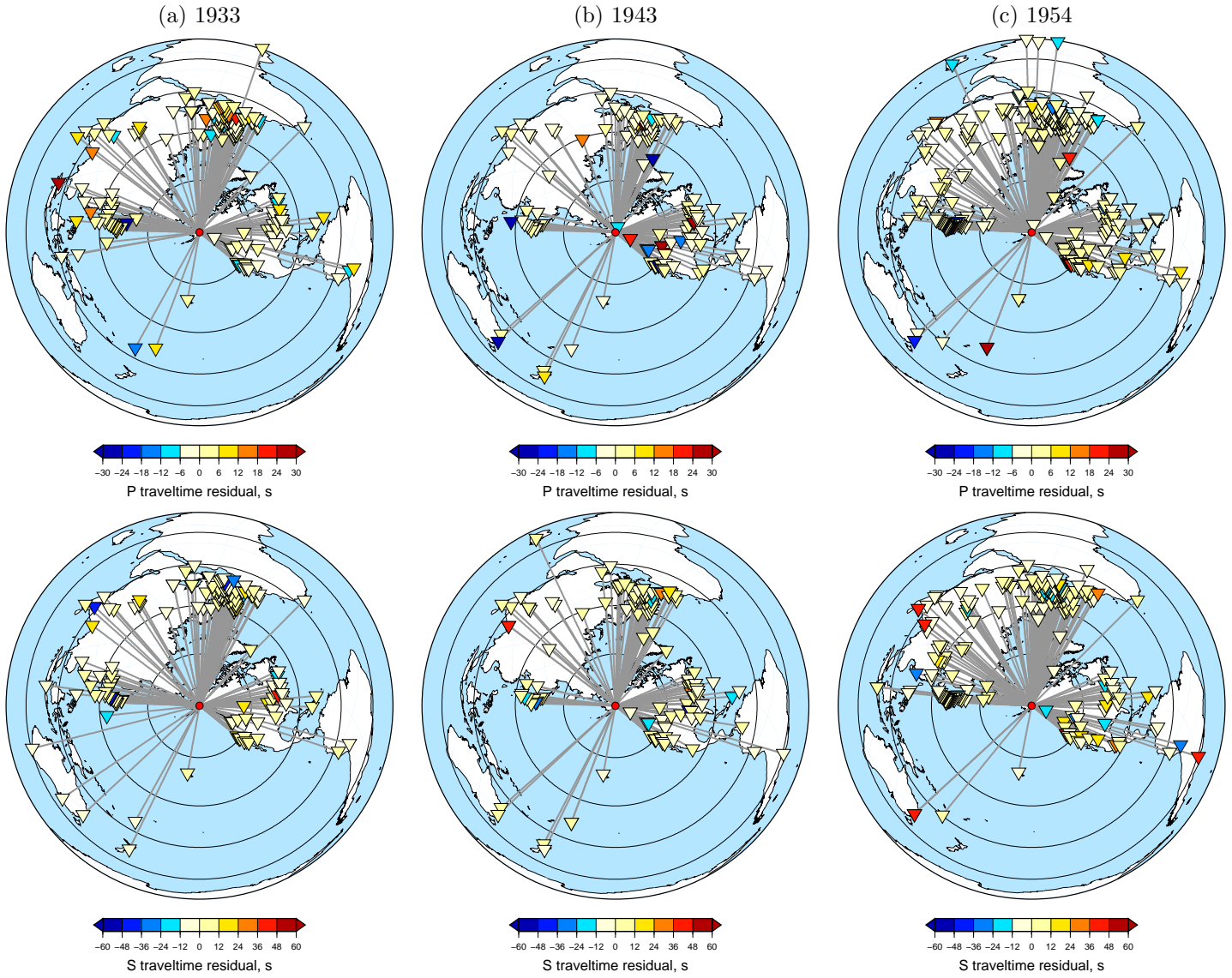


Figure 5: Station coverage for P arrival times (top) and S arrival times (bottom) used in estimating the epicenters for the 1933, 1943, and 1954 Alaska earthquakes. The maximum likelihood epicenter for each earthquake is marked by red circle at the center. The arrival times of the phases were obtained from ISC [42]. The stations are marked by inverted triangles and colored by the difference between the ISC arrival time and synthetic obtained using ak135 velocity model [40]. Circles show epicentral distances of $\Delta = 30^\circ, 60^\circ, 90^\circ, 120^\circ$, and 150° . The posterior epicenters for each earthquake are shown in Figure 6. For details of the results, see [43]. (a) 1933 M_w 6.78 earthquake. There are 174 P arrival times and 158 S arrival times recorded by 179 stations. (b) 1943 M_w 7.34 earthquake. There are 137 P arrival times and 136 S arrival times recorded by 137 stations. (c) 1954 M_w 6.36 earthquake. There are 346 P arrival times and 223 S arrival times recorded by 263 stations.

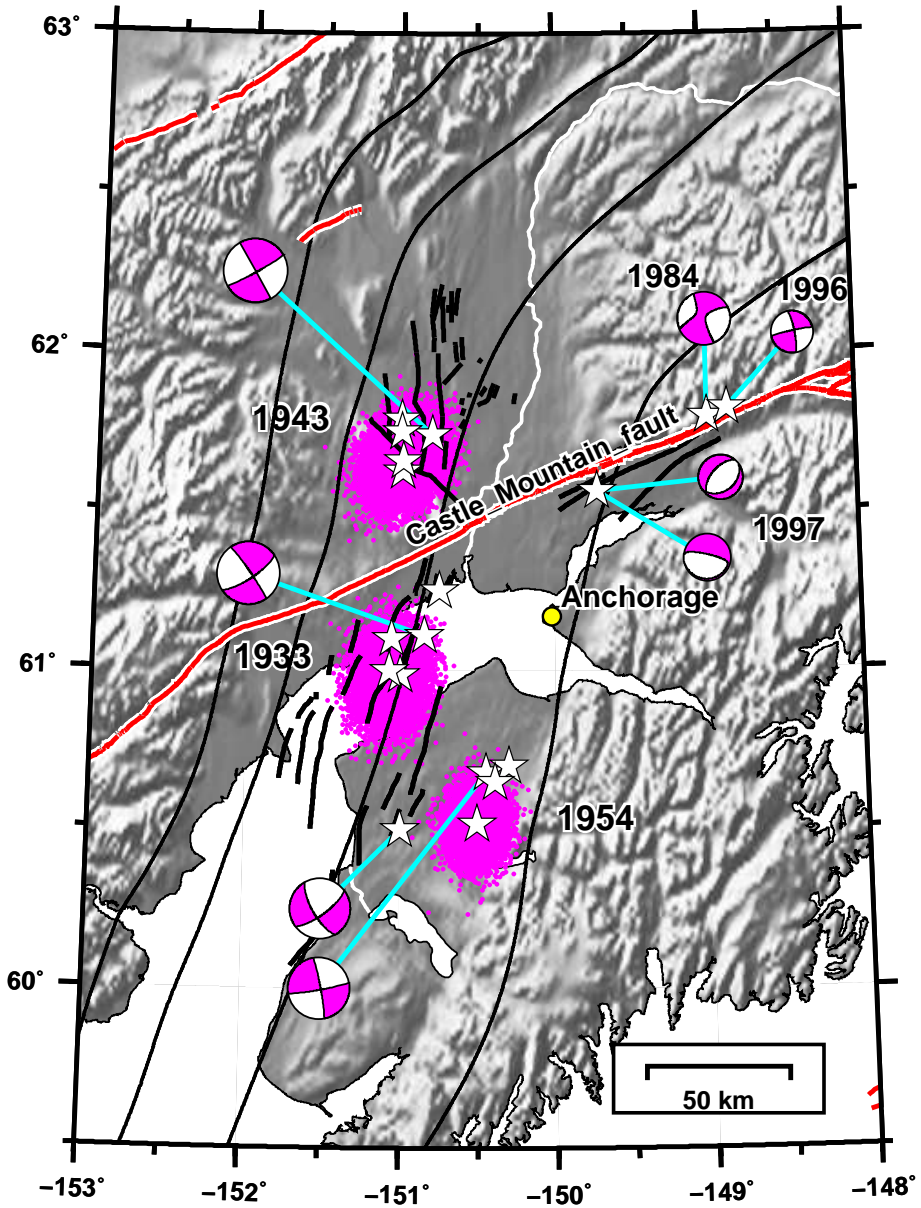


Figure 6: Estimated epicenters for the 1933, 1943, and 1954 earthquakes; see [43] for details. Each cloud of colored dots represents the posterior epicenters, which are centered on a maximum likelihood epicenter (star). Other stars show epicenter estimates from other studies (Table S1: [87, 24, 29, 31]). See Figure 7 for information regarding the depths of the posterior samples relative to the underlying subduction interface. Also shown are active faults and folds [22, 18] and contours of the top of the subducting Pacific plate (40 km, 60 km, 80 km, 100 km) [7]. The beachballs show source mechanisms for 1933 [24], 1943 [24], 1954 [24, 94], 1984 [25], 1996 (AEC), and 1997 (AEC, [25]). The 1984, 1996, and 1997 epicenters are from the AEC catalog.

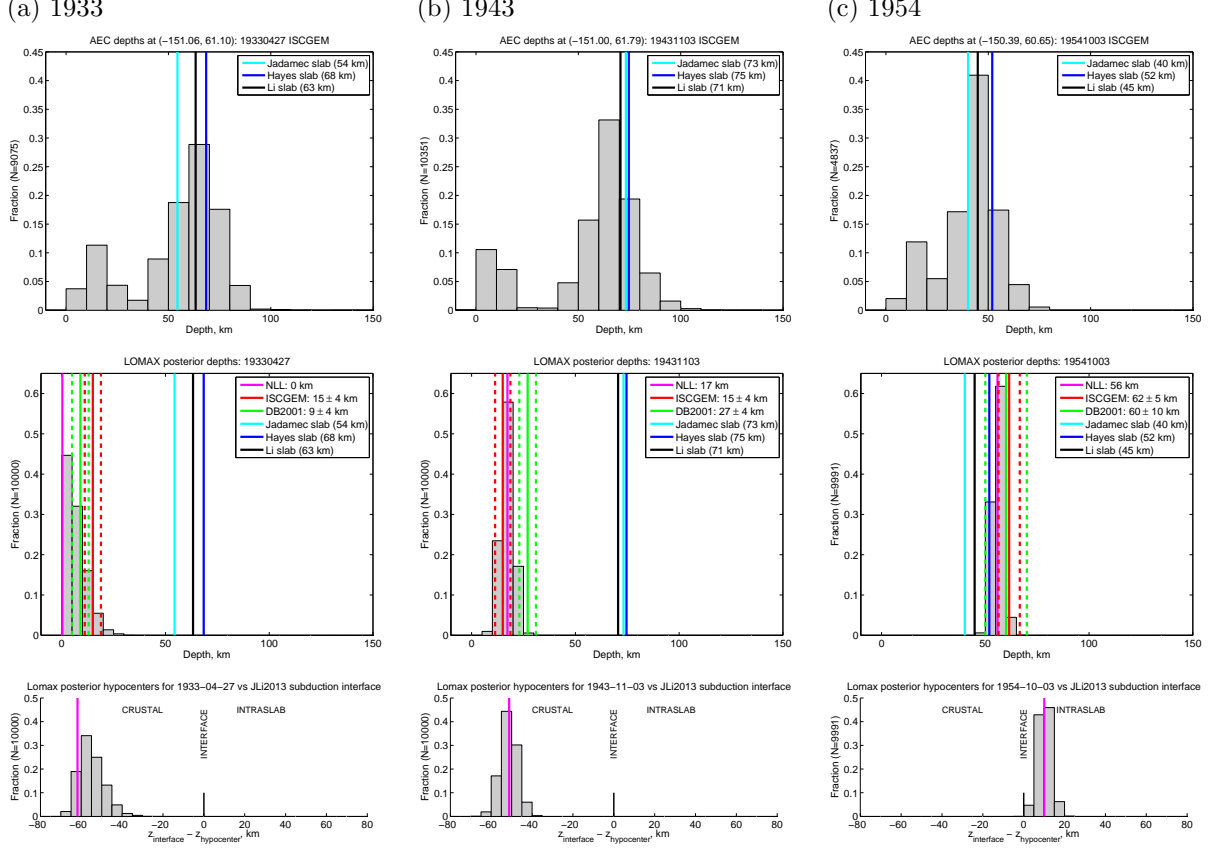


Figure 7: Estimated depth to slab for three historical earthquakes. Each hypocentral estimation using NonLinLoc provides a cloud of posterior hypocenters; see Figure 6 for a map view. For each posterior hypocenter we evaluate the vertical distance to the subduction interface models of [88] (cyan), [89] (blue), and [7] (black). (a) 1933-04-27 M_w 6.8 earthquake. (top) Distribution of depths of modern microseismicity ($M \geq 0$, 2000–2018) whose epicenters are within a 40 km of the ISC-GEM epicenter. (middle) Distribution of depths of posterior hypocenters. Also shown are our maximum-likelihood estimate from NonLinLoc (magenta) and the depth estimates, with uncertainties, from ISC-GEM [31] (red) and DB2001 [24] (green). (bottom) Distribution of vertical distances between our posterior hypocenters and the underlying subduction interface from [7]. Distributions to the left favor a crustal interpretation for the earthquake; distributions to the right favor an intraslab interpretation. (b) 1943-11-03 M_w 7.3 earthquake. (c) 1954-10-03 M_w 6.4 earthquake.

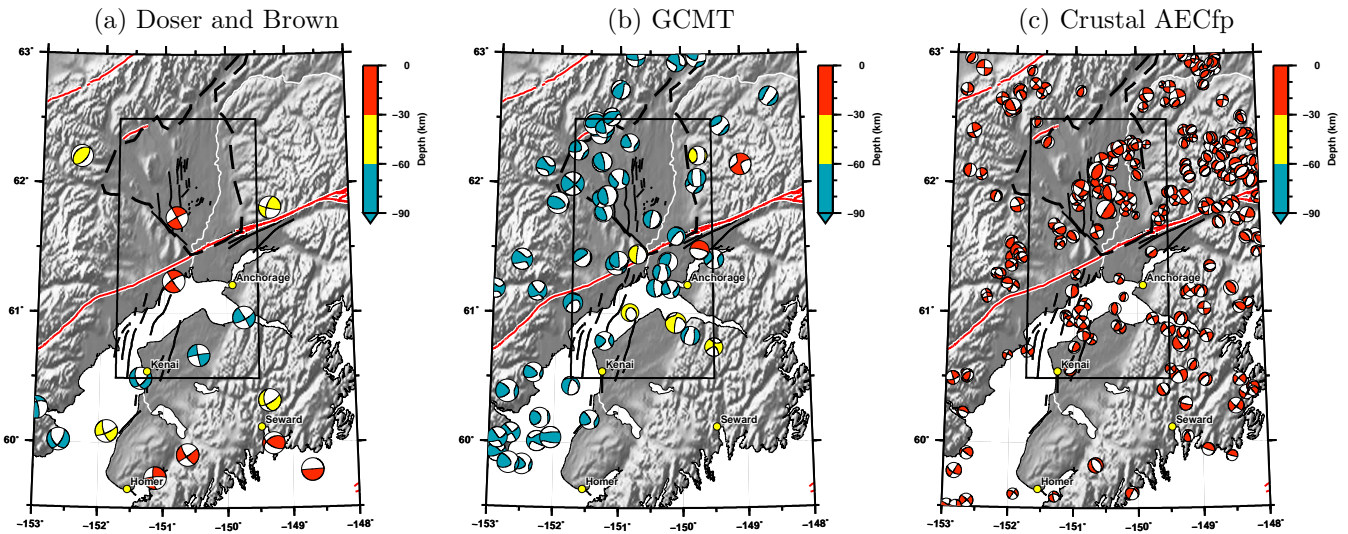


Figure 8: Moment tensor solutions from previous studies. (a) Major historic events (1920–1964), from [24]. The three earthquakes near longitude -150° are, from north to south, the 1943, 1933, and 1954 earthquakes. (b) All events from the GCMT catalog, 1976–2017 [25, 26]. (c) All crustal ($\text{depth} \leq 30 \text{ km}$) events (1990-01-01 to 2017-01-01) from the Alaska Earthquake Center fault-plane catalog. These focal mechanisms are derived from P polarity observations. See Section 2 for more information on major historic events. See Figure 12 for our new moment tensor solutions.

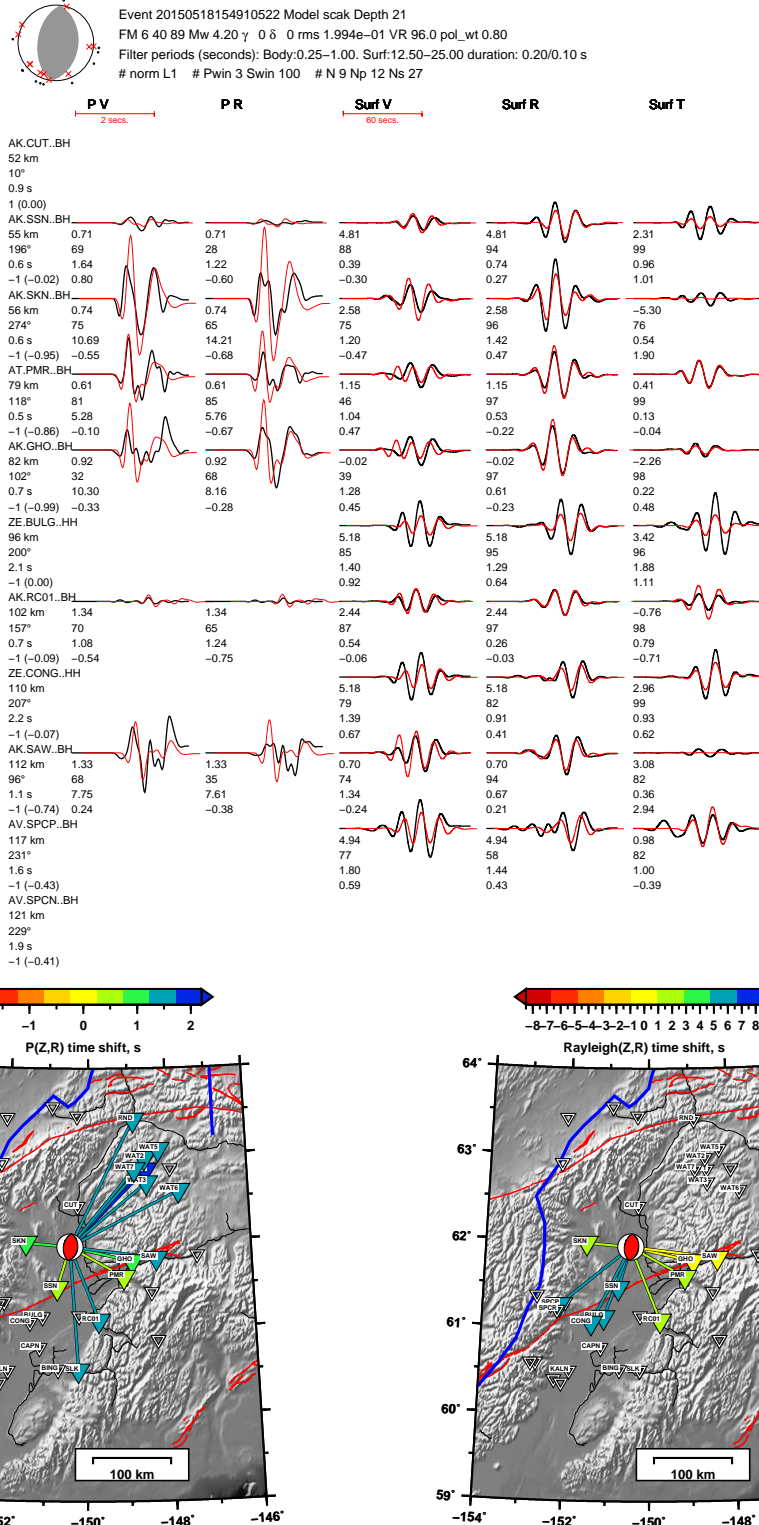


Figure 9: (top) Waveform fits at subset of stations used for a M_w 4.2 crustal earthquake in the Susitna region. See Table S4 for source parameters. Waveform fits for all stations, and for all events, are available [62]. (bottom) Map of time shifts between observed and synthetic waveforms for the P waves (left) and Rayleigh waves (right). Open triangles denote stations with available waveforms that were not used in the inversion. Station names are listed if either the waveform or first-motion polarity was used. Note the large positive time shift for Rayleigh waves traveling to the southwest, through basins. This indicates that along these paths the assumed 1D model is too fast relative to the actual Earth structure.

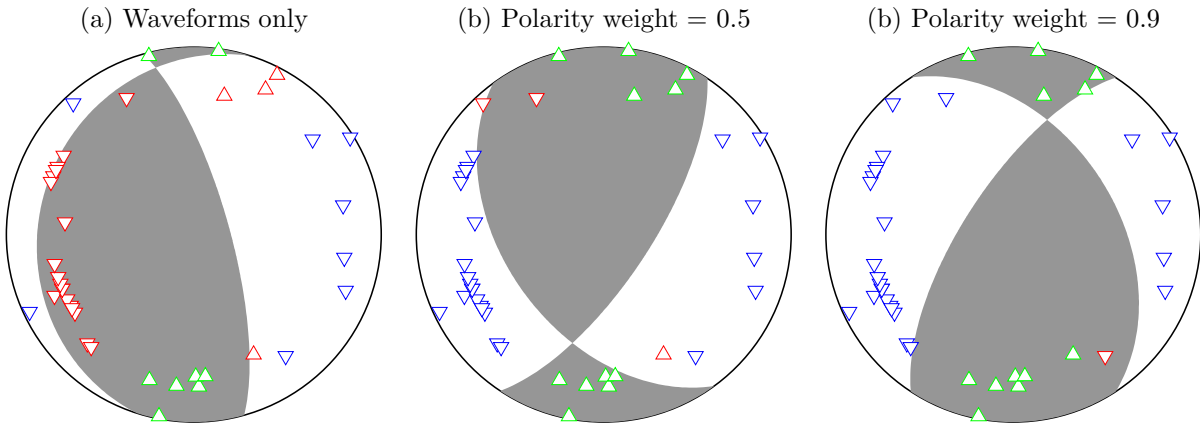


Figure 10: Impact of using different weights for the polarity misfit, shown for an example earthquake in Cook Inlet (eid 20150727022154395). Each beachball shows the best-fitting moment tensor for a given m in Eq. 3. Triangles denote lower-hemisphere piercing points for each ray path from source to station; these are calculated using an assumed 1D Earth model. Upward triangles denote upward polarity observations; downward triangles denote downward polarity observations. The color indicates agreement or not with predicted polarities: red (up or down) indicates mismatch, while green (up) and blue (down) indicate agreement. See Section 3.3 for details on the misfit function. (a) Waveforms only. Note that a large number of polarity mismatches occur. See Figure S5 for waveform fits. (b) Waveforms plus polarities with weight factor 0.5. Here only three polarity measurements are mismatched. See Figure S6 for waveform fits. (c) Waveforms plus polarities with weight factor 0.9. All observed polarities are fit, except one (in red). See Figure S7 for waveform fits.

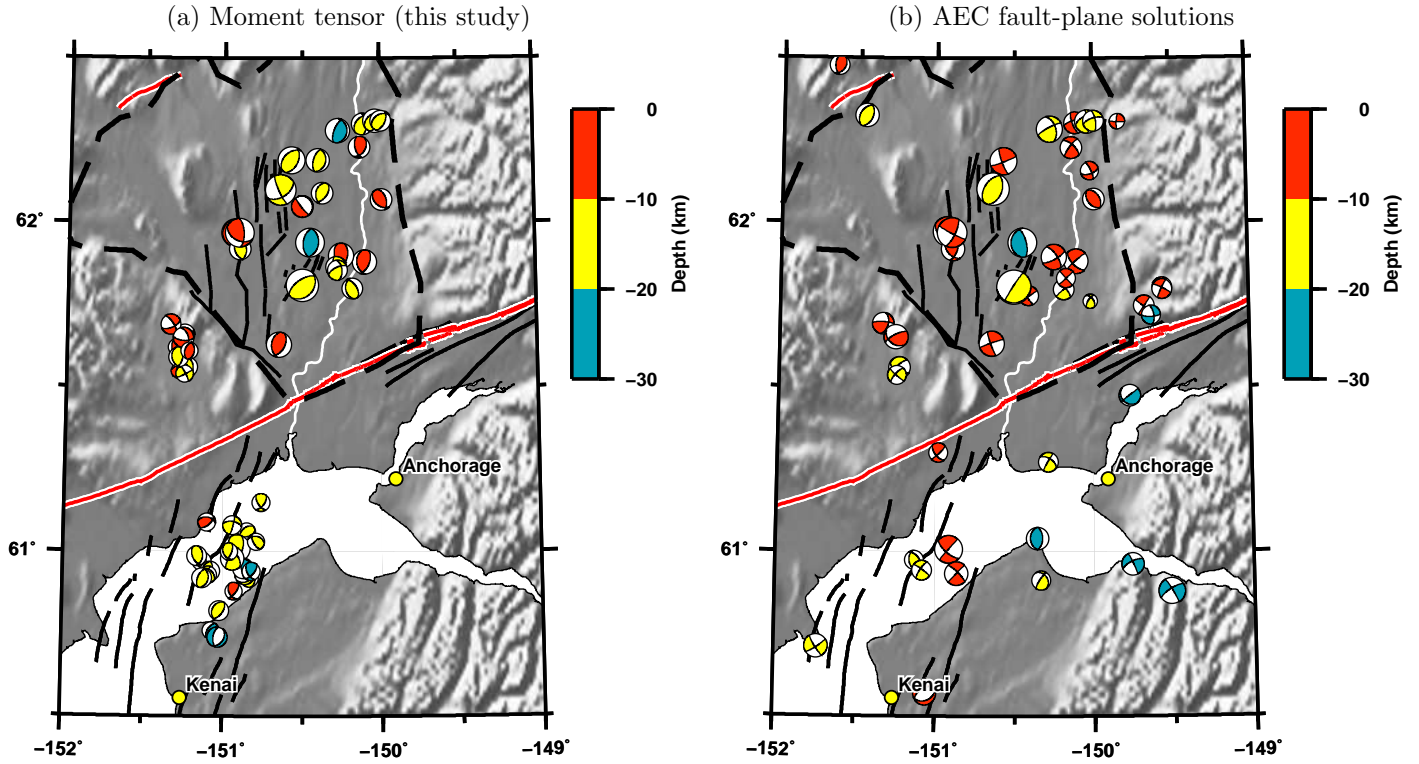


Figure 11: Comparison between moment tensors in this study and an existing catalog. All earthquakes shown are for depth ≤ 30 km and between 2007-08-15 to 2017-01-01. (a) Moment tensors estimated in this study: 53 total, 26 of which are in (b), 27 which are new. These mechanisms are estimated from waveforms and first-motion polarities. (b) Moment tensors in the Alaska Earthquake Center fault-plane catalog: 46 total, 26 of which are in (a), 20 of which we do not examine. These mechanisms are estimated from first-motion polarities.

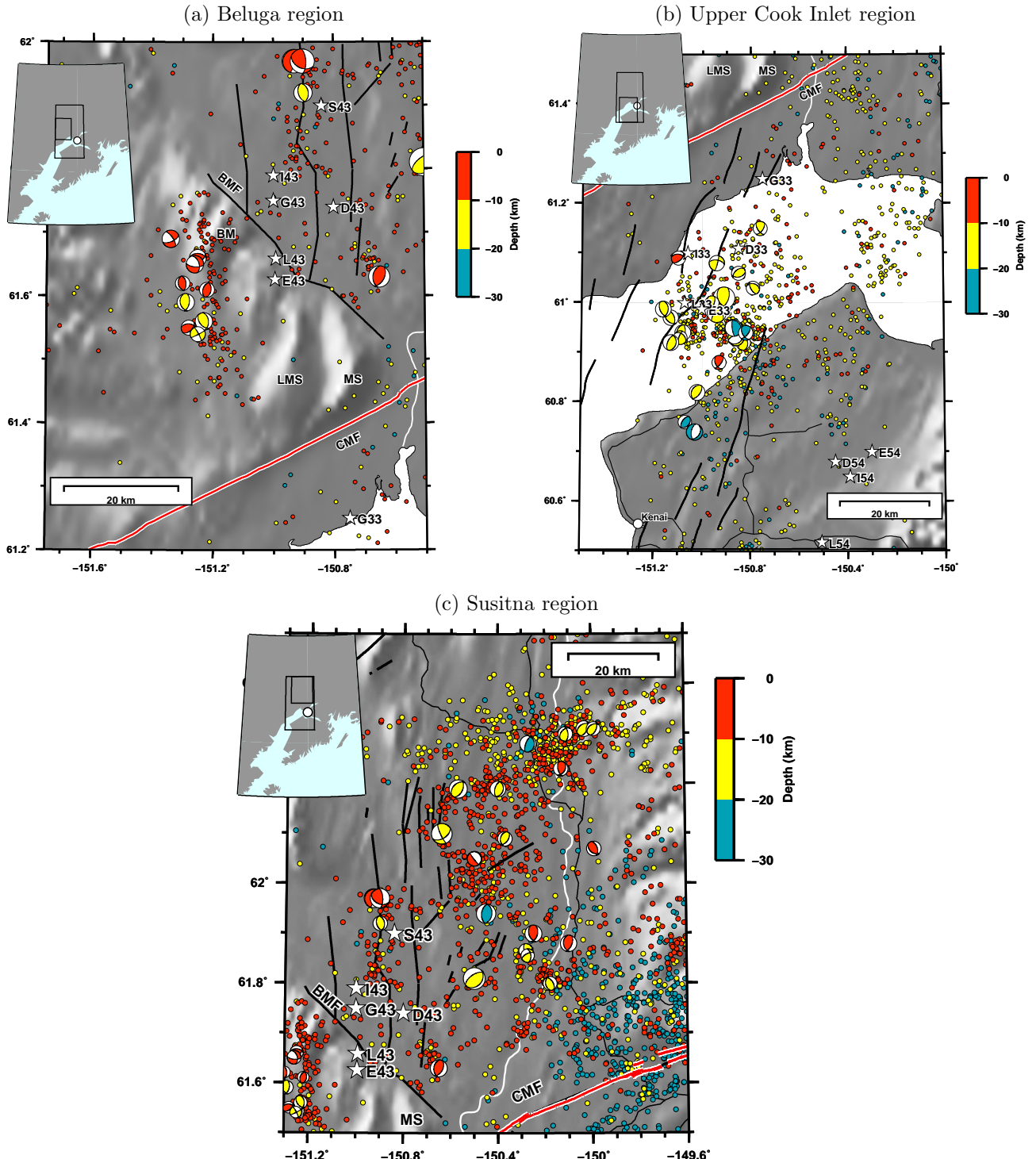


Figure 12: Our double couple moment tensor solutions for crustal earthquakes (depth ≤ 30 km) between 2007-08-15 and 2017-01-01 in three focus regions (Table 1). The displayed regions are slightly larger than the bounding regions listed in Table 1. Beachballs are colored by depth and sized by earthquake magnitude. Also shown are relocated seismicity (Figure 13) and previously published epicenters for the 1933 and 1943 earthquakes, plotted as stars (Table S1). Text labels: CMF = Castle Mountain fault, BMF = Beluga Mountain fault, BM = Beluga Mountain, LMS = Little Mount Susitna, MS = Mount Susitna. (a) $M_w \geq 2.5$ in the Upper Cook Inlet region. (b) $M_w \geq 2.5$ in the Beluga region. (c) $M_w \geq 3.0$ in the Susitna region. See Figure S11 for an alternative version of this figure that includes the basement surface.

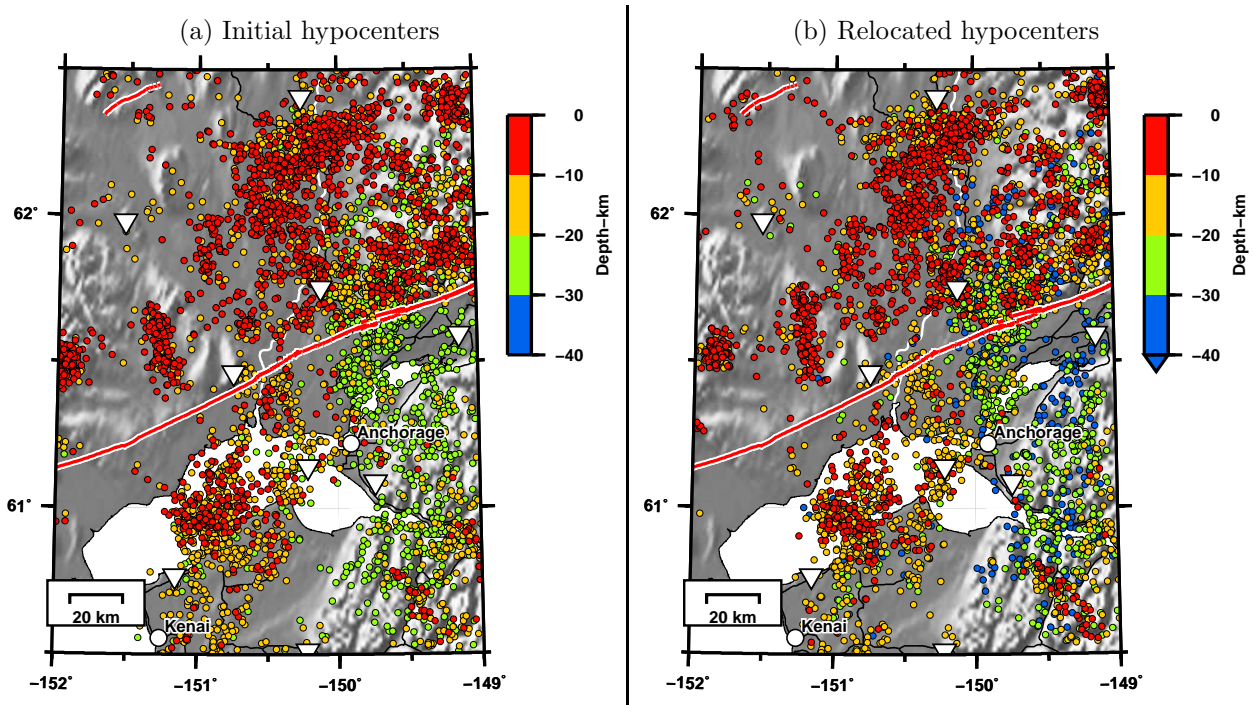


Figure 13: Relocation of hypocenters using a double-difference approach. The crustal earthquakes considered have depth ≤ 30 km, $M_w \geq 1.5$, and occurred between 1990-01-01 and 2017-01-01. See Section 4 and Figure S13 for details.

663 Appendix A. Summary of felt reports for 1933, 1943, and 1954 earthquakes

664 Here we summarize the entries for the 1933, 1943, and 1954 earthquakes within the annual earthquake
665 volumes of the U.S. Coast and Geodetic Survey [95, 96, 97]. See felt report locations on maps in Figure S14.

666 1933-04-27 M_w 6.8

667 The complete entry in [95]:

668 *April 26:* 16:36*. Instrumental epicenter 62° north, 151° west. Anchorage, VI. Telegraph lines
669 were down for a distance of 50 miles from Anchorage. The shock lasted about 3 minutes. Plate
670 glass windows in several stores were broken and stocks of good tumbled from their shelves. This
671 earthquake was considered by residents as the worst in 30 years.

672 The quake was felt strongly on Kodiak Island and along the Aleutian Islands. It was felt strongly
673 at Curry, McGrath, Seward, and Wasilla; Dillingham (Kanakanak), IV; reported light at Healy.
674 The shock was felt at College, Fairbanks, Susitna, Valdez, and Whale Island.

675 Because of the difficulty in correlating the times of occurrence of the following aftershocks it has
676 been considered best to list them all as individual shocks, even though it is evident that this is
677 not always true.

678 *April 26:* Homer; earthquake and following tremors.

679 *April 26:* Kaslif;

680 *April 26:* Big Susitna River District, VII.

681 *April 26:* Old Tyonek, VII. Houses shaken off foundations.

682 1943-11-03 M_w 7.3

683 The complete entry in [96]:

684 **November 3:** 04:32.3.* Anchorage. Sharp shock with abrupt heaving motion made doors swing
685 and windows rattle. Generally felt. A light after-shock occurred at 05:40. Several slight tremors
686 were felt at intervals until about 07:30. Pen on recording rain gage made mark about $\frac{3}{4}$ inch
687 wide at time of main shock. Similar marks were recorded on the barograph traces. Epicenter
688 probably near 62° north, 151° west.

689 Felt at McGrath 04:33. Slight shock reported by Weather Bureau Observer as continuing for
690 about fifteen seconds. "Wall clocks in the Civil Aeronautics Administration and Weather Bureau
691 Offices were stopped. The barograph trace showed no indication of the quake . . ."

692 Felt at Bethel 04:37. Tremors lasting 20 seconds were felt by several. Faint rumbling underground
693 and moderately loud cracking of ice was heard. Building swayed. "The noise moved down the

694 river quickly and then seemed to pass under the station making the earth tremble comparable
695 to a locomotive passing. The ice in the river made a cracking noise for about an hour after the
696 tremors, which lasted about 20 seconds.”

697 Following [96], [44] lists only three felt reports (Anchorage, McGrath, and Bethel), but we found 10
698 additional felt reports within the monthly weather records. Furthermore, p. 4 of the 1943-11-03 Fairbanks
699 Daily News-Miner had an article headlined “Big Quake Felt Here This Morn”. We speculate that the
700 shortage of reports in [96] was due to the national focus on WWII, which may have limited other duties
701 such as earthquake compilations.

702 1954-10-03 M_w 6.4

703 The complete entry in [97]:

704 **October 3:** 01:18:46*. Epicenter $60\frac{1}{2}^\circ$ north, 151° west, Kenai Peninsula, W. VIII. A sharp
705 earthquake rocked a 1,000 square mile area of the lower Alaska mainland. Concrete walls cracked;
706 plaster showered down; plate glass windows shattered; merchandise toppled from shelves at An-
707 chorage, Homer, Kenai, Seward, Sterling, and Valdez. Minor landslides spilled down on the
708 Seward-Anchorage highway. More than 140 feet of railroad tracks were knocked out of commis-
709 sion just north of Potter. Residents on top floors in Anchorage’s two 14-story “skyscrapers” fled
710 into the streets when the violent rocking broke water connections. At the Denali Theater, where
711 a midnight show was in progress, some 850 patrons rushed toward the exists [sic], climbing over
712 seats in a frenzy to escape. Three persons were reported injured slightly in the rush. Motorists
713 driving cars at the time of the quake said it felt “like moving along on a flat tire.” It was also
714 felt at Cordova, Eklutna, Fairbanks, Kaslof, Kodiak, Latouche, Mantanuska [sic] Agricultural
715 Experiment Station, Moose Pass (severe enough to shake things from the shelves), Palmer, Pun-
716 tilla, and Yakutat. Five aftershocks of a few seconds duration followed the main quake at 02:43,
717 05:21, 05:34, 06:18, and 07:26.

718 The MMI VIII shaking intensity for the 1954 M_w 6.4 earthquake was the largest ever reported on the western
719 Kenai Peninsula (Homer, Kenai, Sterling)—even exceeding the MMI VII of the 1964 M_w 9.2 earthquake [44].